Qualitative and quantitative diagenetic modelling in a tight carbonate reservoir in north-western Iraq

Omar K. Mohammed-Sajed[a,b], Paul W. J.Glover[b], Flyah H. Al-Khatony[a], Richard E. Ll. Collier[b]

[a]*Department of Geology, College of Science, University of Mosul, Iraq.*
[b]*School of Earth and Environment, University of Leeds, UK.*

Abstract. The diagenetic history of the Butmah Formation (Lower Jurassic) is very complex and affected by several diagenetic processes that worked effectively with fracturing control to create the final pore network. A microscopic study, core plug and well log analyses were combined in this study in order to describe, and differentiate between, the diagenetic and fracturing control that created the final pore system of the formation. The diagenetic processes of the Butmah Formation were studied in depth to describe the diagenetic stages and identify the elements that may compose a petrodiagenetic pathway illustrating its effect on the reservoir quality of the Butmah Formation. Accordingly, the Butmah Formation samples were divided into three petrophysical fields controlled mainly by fracturing and diagenesis, which were then used to develop a new method for estimating the pre-dolomitisation petrophysical properties of the dolomite samples and the post-dolomitisation petrophysical properties of the limestone samples. Consequently, the output of applying this method allows us to effectively begin to predict each of the elements that may compose a petrodiagenetic pathway for the Butmah Formation and make its reservoir characterisation integrated and more understandable. The new method provided a good prediction of matrix porosity and permeability, as well as allowing the estimation of reservoir properties of any other carbonate reservoir in petroleum development projects when there are no core samples in some formation intervals within boreholes.

Keywords: Diagenetic control, carbonate reservoir, Butmah Formation, poroperm relationship, tight carbonate, petrodiagenetic pathway

1. INTRODUCTION

It is very important to take account of diagenetic processes when considering reservoir quality during exploration studies because of their critical influence on all aspects of the rock microstructure including porosity, pore and pore throat size distributions, pore connectivity and, consequently, permeability (Nader, 2017; Worden et al., 2018; Adelinet et al., 2019; Wang et al., 2019; Baqués et al., 2020; Rashid et al., 2022).

Primary porosity is high in carbonate during deposition, and subsequently modified by diagenesis and fracturing controls (Longman, 1980; Moore, 1989; Ehrenberg, 2004; Scholle and Ulmer-Scholle, 2003; Ahr, 2008). Most, sometimes all, of carbonate rock pores are secondary in origin, having been formed during diagenesis. Consequently, a good understanding of the diagenesis a carbonate rock has undergone is crucial to the interpretation of their petrophysical properties (Selley, 2000; Ahr, 2008; Boggs, 2009; Esrafili-Dizaji and Rahimpour-Bonab, 2009; Tavakoli et al., 2011; Hollis, 2011; Leonide et al., 2014; Zhang et al., 2017; Nader, 2017; Mohammed Sajed and Glover, 2020). Depositional control should also be considered as a benchmark to improve understanding the role of diagenetic processes and fracturing in improving or reducing the carbonate reservoir quality (Hollis et al., 2010; Agar and Geiger, 2014; Shuja Ullah et al., 2023).

Diagenesis and fracturing can occur *in tandem* to improve or reduce the reservoir quality of carbonates (Moore, 2001; Ahr, 2008). Rocks are affected differently by fractures depending on their type, nature, and severity inside the rock (Caine et al., 1996; Childs et al., 1997; Maerten et al., 2002; Geraud et al., 2006; Laubach et al., 2019; Corrêa et al., 2022; Forstner and Laubach, 2022; Rysak et al., 2022; Wang and Laubach, 2023). In carbonate rocks, fractures occur to variable degrees and, if open, enhance fluid movement and the quality of the reservoir (Arosi and Wilson, 2015; Wennberg et al., 2016; Mohammed Sajed and Glover, 2020; de Lima et al., 2023). If cemented, fractures can hinder fluid flow and compartmentalise reservoirs (Mohammed-Sajed and Glover, 2022).

The type and degree of diagenetic processes both significantly affect the distribution of pore-throat sizes, bulk, potential, and effective porosity, as well as permeability, and other petrophysical parameters through their ability to create, enhance, rework, occlude, and destroy pores in carbonate rocks (Tavakoli et al. 2011; Wang et al., 2019; Mohammed Sajed and Glover, 2020; Mohammed Sajed et al., 2021; Rashid et al., 2022).

Diagenesis has been investigated intensively in many studies (e.g., Bourque et al., 2001; Cerepi et al., 2003; Stentoft et al., 2003; Esrafili-Dizaji and Rahimpour-Bonab, 2009; Maliva et al., 2009; Tavakoli et al., 2011; Hollis, 2011; Leonide et al., 2014; Zhang et al., 2017; Jiang et al., 2018). These studies have all been qualitative, focussing on the use of observations of morphological changes to characterise the type, extent and conditions involved in the diagenetic processes, and their effect on the porosity of the rock. The diverse porosities and pore types of many carbonate reservoirs are caused by intricate diagenetic mechanisms. Understanding the likely products of each diagenetic process is necessary in order to comprehend the petrophysical characteristics of the resulting carbonate reservoir (Longman, 1980; Tucker et al., 1990; Anselmetti and Eberli, 1993; Moore, 2001; Boggs, 2006 and 2009; Verwer et al., 2008; Brigaud et al., 2010).

Recently, there has been progress in understanding tight carbonate rocks better by using carbonate petrophysics to make the understanding of diagenesis more quantitative (Rashid et al., 2015a; 2015b; 2017; 2022; Al-Khalifah et al., 2020; Sabouhi et al., 2022; Glover et al., 2022). Rashid et al. (2015a; 2015b; 2017), for example, have produced methods for estimating permeability in carbonates. Integrated analysis of facies, well logs and seismic data were adopted by Sabouhi et al., (2022) as a new approach to quantitative diagenesis modelling in the Sarvak Formation in south-western Iran. Machine learning has been applied to the characterisation of tight carbonates and the recognition of facies caused by diagenetic processes (Al-Khalifah et al., 2020; Glover et al., 2022), while the concept of petrodiagenetic pathways for describing how the quantitative poroperm characteristics of a rock change as a result of concurrent and contemporaneous diagenetic processes is another recent development (Al-Khalifah et al., 2020; Rashid et al., 2022). This emerging field of Quantitative Diagenesis seems to have started well.

The reservoir quality of the Butmah Formation in this study is controlled mainly by diagenetic and fracturing factors. Accordingly, the Butmah Formation represents an exemplar for other formations that show the operation of diagenetic processes working with fracturing to result in the same current rock composition and texture, such as the Khuff, Dalan, and Kangan formations in the Middle East (Alsharhan, 2006; Ehrenberg et al., 2007; Koehrer, et al., 2010; Tavakoli et al., 2011; Aleali et al., 2013; Amel et al., 2015).

This study shines a light on how to differentiate between diagenetic and fracturing controls using qualitative and quantitative methods in order to identify the effect of each control on the petrophysical properties of the Butmah Formation. This new method can also be applied to other carbonate formations in order to estimate of the porosity and permeability of a dolomite if the petrophysical properties of the pre-dolomitised limestone are known. Conversely, the method can be used to estimate the porosity and permeability of the pre-dolomitised limestone from knowledge of the petrophysical properties of the existing dolomite.

The new method represents a very useful approach for fast and effective prediction of the porosity and permeability of any carbonate reservoir consisting of both limestone and dolomite lithology, especially if there is a shortage of core samples within boreholes. Moreover, this method will help to create its petrodiagenetic pathway and make its reservoir characterisation integrated and more understandable.

2. BACKGROUND OF THE STUDY AREA AND FORMATION

This paper describes the Butmah Formation as encountered within the Ain Zalah and Butmah oilfields north-western Iraq.

The Ain Zalah anticline is located in the Zagros foothills zone, about 60 km north-west of Mosul city in northern Iraq. On the surface, it is represented by a long, low topographic high that is approximately 20 km long by 5 km broad and has a maximum elevation of 457 m above sea level. The Butmah anticline runs parallel to and south-east of the Ain Zalah anticline. It is a 12 km long and 6 km broad asymmetrical anticline made up of two domes, one eastern and one western (Dunnington, 1958; Bellen et al., 1959; Hart and Hay, 1974) (Figure 1). Oil is extracted from fractured limestones of the Shiranish Formation (Campanian-Lower Maastrichtian) in both anticlines. In addition, limited oil production occurs in some wells from the Mauddud (Albian), Butmah (Lower Jurassic), and Kurrachine Formations (Upper Triassic) (Aqrawi et al., 2010).

Figure 1. The position of the Butmah and Ain Zalah oilfields in north-western Iraq may be observed along with the tectonic division of Iraq after Fouad (2015).

Dunnington (1953) identified the Butmah Formation at Butmah oilfield in north-western Iraq as a 500 m thick, high heterogeneity carbonate unit (Bellen et al., 1959), while the authors of this paper (Mohammed Sajed and Glover 2020; Mohammed Sajed et al., 2021; Mohammed-Sajed and Glover, 2022) characterised the examined section (Butmah-15) as five stratigraphic units including three primary lithofacies (Figure 2). Limestone alone or associated occasionally with anhydrite nodules makes up Lithofacies 1, which is numerous times reiterated as units 1, 3, and 5 (U1, U3, and U5). Shale and a few anhydrite nodules interbedded the dolomite in Lithofacies 2. Dolomite with beds and nodules of anhydrite make up Lithofacies 3. Unit 4 is the only one that represents it.

Figure 2. Stratigraphic units, lithofacies, microfacies distribution, and environments of the Butmah Formation at well Bm-15.

These identified stratigraphic units of the Butmah Formation were subdivided into eight microfacies, which were used to identify the palaeo-environment of the formation into; (i) tidal flats, (ii) lagoon, and (iii) shoal (Figure 2). The tidal flat environment is characterised by the presence of crystalline anhydrite (B1), nodular dolomudstone (B2), and dolomudstone with sparse anhydrite crystals (B3). The lagoon environment is characterised by dolomudstone with sparse anhydrite crystals (B3), stromatolite boundstone (B4), fossiliferous packstone (B5), and peloidal wackstone/packstone (B6). Finally, the shoal environment is represented by peloid-ooidal packstone (B7) and ooidal grainstone (B8) microfacies (Mohammed-Sajed and Glover, 2022).

3. MATERIALS AND METHODS

3.1 Wireline log data

A limited set of wireline log data (gamma ray, density, neutron, and sonic logs) from two wells, Bm-15 and Az-29, located in the Butmah and Ain Zalah oilfields, respectively, were provided by the North Oil Company (NOC) in Iraq. The Interactive Petrophysics® software (version 4.3) from Senergy® Inc. was used to redraft and analyse these well logs after they had been digitally converted using Didger® software (version 3.5). The Butmah Formation's porosity has been determined using wireline log data, which has also been utilised to distinguish between diagenetic and fracturing controls. Furthermore, the wireline log data has been merged with core descriptions in order to identify lithofacies describing the stratigraphic units of the Butmah Formation (Mohammed Sajed and Glover, 2020).

3.2 Image analysis

Microscopic description of rock microstructure using thin sections and petrological, binocular or scanning electron microscopes is one of the most important tools for the determination of the mineralogy of its components and the porosity and pore structure of its pores (micro-texture). These features are crucial for determining the rock's origin, depositional facies, deposition environment, and the type, degree, and timing of any diagenesis that has occurred. (Flugel, 2010).

Under the binocular microscope, 540 thin-section slides were examined to characterise the depositional facies and environments, diagenesis, and pore network of the Butmah Formation. Alizarin red (AR), potassium ferricyanide ($K_3(FeCN)_6$), and hydrochloric acid (HCl) were used to stain all thin-section slides made from cores, according to Dickson's (1965) staining procedure. This was carried out in order to distinguish between carbonate minerals such as calcite, ferroan calcite, and dolomite. Prior to the production of thin sections, an epoxy containing blue dye was injected into the rock to emphasise the pores in the thin section slides.

Sixteen samples were selected from the Butmah formation for imaging at a nanometer scale size using Scanning Electron Microscopy (SEM). The SEM analysis was used to identify the sample components (grains, crystals and pores) under high magnification of up to 10,000×, allowing resolutions down to 50 nm.

Solvents were used to clean all of the selected samples to remove any hydrocarbon residue or dust that may have compromised the picture quality (Erdman and Bell, 2015). After drying the samples, some of them were polished, whereas others were left with a fresh broken surface to obtain three-dimensional image of the broken surface. The samples were then placed on stubs and covered with a 20 nm layer of carbon for image capturing (Erdman and Bell, 2015).

3.3 Porosity and permeability

A total of 84 core plug samples with nominal dimensions of 1.5 inches in diameter and 2.0 inches in length were measured by the Wolfson laboratory at the University of Leeds. After utilizing Soxhlet extraction to clean them, the samples were dried for 48 hours in a temperature-controlled oven at 60°C (McPhee et al., 2015). Helium pycnometry was used to determine the porosity of each dry sample at a pressure of 15 psig (Spain, 1992).

For samples with high permeability (k > 1 mD), a steady-state method was used (Ross, 2011), and for samples with lower permeability (k<1 mD), a pulse-decay permeameter was used (Jones, 1997; Jannot et al., 2007; Zhang et al., 2000; McPhee et al., 2015). Both methods used helium as the probe gas. The Klinkenberg adjustment was applied to all the measured samples to correct for so-called gas "slippage," which occurs when the criterion for continuity in the gas fails (Klinkenberg, 1941; Rushing et al., 2004; Haines et al., 2016). A further set of data for 16 samples, that were provided from the NOC, included porosity measurements as well as estimated permeabilities of fractured samples using the empirical equations of Ross (2011).

3.4 Pore throat description

According to their lithology, porosity, and permeability, eight samples were chosen for the mercury injection capillary pressure (MICP) test in order to describe their pore-throat size distributions using pressure up to 60,000 psig, applying the Young-Laplace equation (Washburn, 1921; Jennings, 1987; Kopaska-Merkel and Amthor, 1988; Katz and Thompson, 1987; Glover et al., 2006). The samples were cleaned and evacuated after slicing to sizes between 15 and 10 mm. A Micromeritics Autopore IV 9250 device was then used to collect the mercury intrusion data (Giesche, 2006). The approach developed by Glover and Déry (2010) was used to calculate characteristic pore size distributions.

4. DIAGENETIC AND FRACTURING CONTROLS

Based on the petrographic study of the Butmah Formation, three diagenetic stages have been distinguished, belonging to the three digenetic realms; marine, meteoric and burial. These stages are discussed below with details about their petrographic evidence and interpretation.

4.1 Stage 1 (*marine and syn-depositional diagenesis*)

This stage is represented by microbial micritisation, marine cementation, light mechanical compaction, and early anhydrite cementation (Scholle and Ulmer Scholle, 2003; Ahr, 2008; Boggs, 2009).

Micritisation is shown in most packstone and grainstone microfacies of the Butmah Formation. Some skeletal grains show a thin black micritic envelope coating around the grains. The micritic envelope is sometimes still discernible even after the grain has been disintegrated (Figure 3A).

In the oolitic grainstone of the Butmah Formation, isopachous calcite cement with a bladed rind can be found either directly on the ooids or in its micritic envelope (Figure 3B). Furthermore, the fibrous cement was found to fill some fractures (Figure 3C).

Anhydrite cementation and the formation of anhydrite nodules of the Butmah formation have occurred in confined, shallow marine settings under hypersaline circumstances (Figure 3D, and 3E). Most of the anhydrite are primary in origin. This is inferred from many features, including early dolomitisation accompanied by this anhydrite cements, the usual structure of this diagenetic realm comprises interactions between anhydrite and dolomite, cross-cutting of anhydrite with stylolites, and poikilotopic anhydrite that fills intergranular porosity (Figure 5F).

Figure 3. Observed textures associated with diagenetic processes. (A) Micritic envelops around skeletal grains (ooids), Bm-15, (2627 m). (B) Isopachous cement, Bm-15, (2540 m). (C) Fibrous cement, Bm-15, (2480 m). (C) Blocky cement, Bm-15, (2524 m). (D) Anhydrite nodules in fine dolomite crystals, Bm-15, (2500 m). (E) Spare anhydrite crystals in Dolomudstone microfacies, Bm-15, (2350 m). (F) Poikilotopic anhydrite cement, Bm-15, (2292 m). (G) A low peak amplitude stylolite (pressure solution) within fine crystalline dolomite, Bm-15, (2391m). (H) Slightly-compacted contacts between dolomitised peloids, Bm-15, (2541 m). (I) Fine crystalline dolomite showing vuggy porosity and solution-enlarged vugs Bm-15, (2391 m). (J) Drusy cement, Bm-15 (2290 m). (K) Mechanical compaction between ooids within ooids grainstone microfacies, Az-29, (3358 m). (L) A high peak amplitude stylolite (pressure solution) within fine crystalline dolomite, Bm-15, (2378m). (M) Zoning coarse dolomite crystals as late dolomitisation features, Bm-15, (2376 m). (N) Late-stage anhydrite cement occluding early porosity, Bm-15, (2390 m). (O) Compressed chicken-wire texture by compaction effect, Bm-15, (2379 m). (P) Late-stage blocky anhydrite cement fills some fractures and alongside stylolite, Bm-15, (2524 m). (Q) Burial dissolution as a few voids and solution enlarged stylolite, Bm-15, (2381 m). (R) Two generations of fractures, the old fracture is occluded by blocky anhydrite cement and the new open fracture cuts the old one, Bm-15, (2524 m).

Petrographic evidence of syndepositional dolomite were represented by fine to medium euhedral to subhedral crystals of dolomite, preservation of depositional and early diagenetic characteristics such as micritisation and marine cementation. This dolomite is associated with anhydrite fabrics and is cut by stylolites and fractures (Figure 3G). Moreover, slightly-compacted contacts between dolomitised crystals suggest that this dolomitisation occurred before significant burial (Figure 3H).

4.2 Stage 2 (*meteoric and mixing zone diagenesis*)

In this stage, metastable grains are dissolved and generate secondary porosity according to Choquette and Pray (1970). Petrographic evidences for this realm are represented by intergranular/intercrystal dissolution pores and solution-enlarged vugs (Figure 3I).

Furthermore, drusy calcite cement was noted clearly in the Butmah Formation as freshwater cementation (Figure 3J), and mechanical compaction reflects shallow-burial conditions without or with only poorly developed stylolites (Figure 3K).

4.3 Stage 3 (***Burial diagenesis***)

Many of the characterised diagenetic processes in the Butmah Formation are related to this realm such as recrystallization, cementation, chemical compaction (stylolitization) and late dolomitisation (Tucker et al., 1990; Scholle and Ulmer Scholle, 2003; Ahr, 2008).

Chemical compaction is represented by stylolites lines make way for the dissolution fluids that created by the chemical compaction (Figure 3L). Other diagenetic features were also observed, such as; (i) late dolomitisation and saddle dolomite cementation, which occurred during the late burial diagenesis (Figure 3M), (ii) late stage anhydrite cement occluding early porosity and late fractures (Figure 3N), (iii) Anhydrite textures previously created were compacted into chicken-wire anhydrite after burial (Figure 3O), (iv) late-stage anhydrite forms filling some fractures and alongside stylolites in some places as a blocky or granular cement (Figure 3P), and finally (v) burial dissolution, which is usually associated with well-developed chemical compaction units. There were also noted a few cavities, solution-enhanced fractures and stylolites (Figure 3Q).

Fracturing is significant in the Butmah Formation and plays different roles in improving the reservoir properties of each stratigraphic unit depending on whether the presence or lack of anhydrite cement partially or completely occluding fractures (Figure 3R).

Taking all of the previous observations into account, we have created a possible diagenetic sequence for the Butmah Formation, which is shown in Figure 4. In this figure, we have included timing, position (diagenetic environment) of each identified diagenetic stage in this study including their diagenetic processes. Figure 4 also illustrates the effect of diagenesis as an improvement or reduction of the petrophysical properties to create the pore system of the studied formation.

Figure 4. Summaries of the qualitative diagenetic pathway include a generalised diagenetic sequence with the effect of each diagenetic process on the reservoir quality of the Butmah Formation.

5. PETROPHYSICAL PROPERTIES

The petrophysical investigation in this study includes describing porosity, pore throat size and distributions, permeability, and pore size and shape.

5.1 Porosity

The porosity of the rock unit defines its maximum storage capacity. Generally, porosity ranges from little more than 1% for some tight clastic and carbonate reservoirs to a maximum of about 40% for some high porosity carbonate reservoirs (Asquith and Krygowski, 2004; Gluyas and Swarbrick, 2004; Tiab and Donaldson, 2012; Rider, 2018; Mohammed Sajed and Glover, 2020).

In this work, we report effective porosities to helium, which approach the total porosity of the rock because the helium molecule is small enough to access most connected pores, however small. The effective porosity of the studied samples from U4 and U5 are presented in Table 1 and Figure 5. The highest porosity in the dolomite samples (U4) of the Butmah Formation was 8.6%, and the lowest 0.72%, with an arithmetic mean of 4.62%, and a mode of 3.5%. Compared to the U4 measurements, the limestone samples (U5) were shown to have lower porosities, with the highest porosity being 6.91%, and the lowest being 0.19%, with an arithmetic mean 2.72%, and a mode of 1.5%. As expected, the porosity ranges of the limestone and dolomite overlap significantly, but it is the dolomite which presents the larger porosities on average.

Table 1. Statistics of the effective porosity in the stratigraphic units 4 and 5.

Number of samples	**Stratigraphic units**	**Lithofacies**	**Effective porosity (%)**				
			Min	Max	Mean	Mode	Std Dev
36	U.4	L.3	0.72	8.6	4.62	3.5	4.64
31	U.5	L.1	0.19	6.91	2.72	1.5	3.38

Figure 5. The effective porosity histogram of the Butmah Formation at well Bm-15.

Figure 5 illustrates that the Butmah Formation's porosity distribution is roughly unimodal with a wide spread (standard deviation = 4.64% in U4 and 3.38% in U5). Consequently, the effective matrix porosity of all units in the Butmah formation is less than 9%, but varies widely, from 0.19% – 6.91% for the dolomite samples (U4) and 0.72% - 8.6% for the limestone samples (U5).

5.2 Pore throat characterisation

Pore throat size is important because it is related to reservoir porosity, permeability and irreducible water saturation (Porras and Campos, 2001). The variations in pore throat and pore size distribution in the Butmah Formation's limestone and dolomite units are due to dolomite recrystallisation, anhydrite fraction and distribution, and other diagenetic processes (Mohammed Sajed and Glover, 2020). Eight samples were selected for mercury injection capillary pressure (MICP) measurements. Figure 6 displays the pore throat distributions from several of these samples as a result of the MICP study.

The limestone samples (Figure 6A and 6B) exhibit a single peak, but with slightly different styles. Both limestone samples show moderate pore sorting, one with a peak at 7 nm with very few pores larger than 1 µm, the other has a peak at about 30 nm and its largest pore is 600 nm in diameter.

The two dolomite samples are presented in the bottom row of Figure 6. A wider variety of pore diameters may be seen in the dolomite samples, with poor pore sorting, and ill-defined double peaks at 30 nm and 2 µm for Sample C, and 40 nm and 4 µm for Sample D. It is possible that the peak at the smaller size represents relict porosity from before dolomitisation, while the larger pore sizes are all derived from the dolomitisation process.

Figure 6. Pore throat distributions for four samples from the Butmah Formation; top row (A and B) from the limestone lithofacies (U5, L1), and bottom row (C and D) from the dolomite lithofacies (U4, L3).

5.3 Permeability

The permeability of a rock describes its ability to transmit fluid and it is measured in m^2 in SI units or in darcies (D) or millidarcies (mD) in industry (Tiab and Donaldson, 2012). The results of the permeability measurements made in this work are summarised in Table 2 and Figure 7.

Table 2. Permeability measurements of the studied formations.

Units	Lithofacies & lithology	No. samples	Matrix permeability (mD)			
			Min	Max	Geometric Mean	Log-normal measure of standard deviation
U4	L.3 (dolomite)	47	5.41×10^{-5}	6.10×10^{-2}	8.6×10^{-3}	$+7.14\times10^{-7}$ $-1.04\times10^{+2}$
U5	L.1 (limestone)	43	1.30×10^{-6}	7.69×10^{-3}	0.42×10^{-3}	$+2.52\times10^{-10}$ $-7.0\times10^{+2}$

The permeability measurements are not distributed normally, but approximate to a log-normal distribution. Consequently, we have calculated the log-normal arithmetic mean (which is the geometric mean of the raw data) and the equivalent measure of standard deviation. The dolomite samples of the U4 have a unimodal distribution in terms of permeability, with the lowest value being 5.41×10^{-5} mD and the highest being 6.10×10^{-2} mD, with a geometric mean of 8.6×10^{-3} mD and a log-mean standard deviation of $+7.14\times10^{-7}/-1.04\times10^{+2}$ mD. The limestone samples of U5 permeability measurements also show a unimodal distribution but shifted to lower values, the lowest value being 1.30×10^{-6} mD and the highest being 7.69×10^{-3} mD, with a geometric of 0.42×10^{-3} mD and a log-mean standard deviation of $+2.52\times10^{-10}/-7.0\times10^{+2}$mD.

Figure 7 shows that the permeability in the dolomite rocks of the U4 of the Butmah Formation is distributed between 1.0×10^{-1} mD and 1.0×10^{-5} mD, with the highest occurrence (33.3% of the measurements) in the range 1.0×10^{-3} mD – 1.0×10^{-4} mD. By contrast, the permeability measurements of the limestone samples from U5 of the Butmah Formation show fewer values distributed between 1.0×10^{-2} mD and 1.0×10^{-6} mD, with the highest occurrence (48.4% of the measurements) in the range 1.0×10^{-4} mD – 1.0×10^{-5} mD. As expected, the dolomite presents generally higher permeabilities than the limestones, although there is an overlap in the permeability ranges. The reasons for this are (i) dolomites commonly have larger matrix porosity than limestones, and (ii) dolomites are more brittle than limestones, and are consequently more suceptible to the development of permeability-enhancing fractures.

Figure 7. Histogram showing the permeability of the dolomite and limestone lithofacies in the Butmah Formation.

5.4 Pore description

The pore network of the Butmah Formation has been characterised based on optical and SEM microscopy. Units 1, 3 and 5 consist of tight limestones, characterised by small mesopores (1-62.5 μm) as vugs and intergranular porosity (Figure 8A, B, and C). Some of the pores in these units (Lithofacies 1) are occluded by anhydrite and calcite cement.

Units 2 and 4 consist of different kinds of pores within dolomite lithofacies (Lithofacies 2 and 4). These pores are dependent on the crystallisation of dolomite and the formation of anhydrite cement in the spaces between the crystals. These lithofacies have exhibits increased porosity and pore sizes when the anhydrite cement is dissolved as a late diagenetic process, providing large mesopores (62.5 μm – 1 mm) as intercrystalline and separate and/or touching vugs (Figure 8D, E, F, G, H, and I).

All of the characterised stratigraphic units have significant levels of fracture intensity, but most of the fractures are occluded (filled or semi-filled) by anhydrite cement and some calcite cement. Accordingly, there are some open fractures were described especially in units 3, 4 and 5. The final shape of pore network indicates that units 1, 3 and 5 the pore structure is controlled by a combination of dissolution and fracturing, whereas units 2 and 4 are more complex than the other units, with their pore structure controlled by dissolution, dolomitisation and fracturing.

Figure 8. The Butmah Formation pore structures. (A) (B) (C) Stromatolite boundstone microfacies, Bm-15, U4 (2278 m) with (A) intercrystalline porosity and (B) intercrystalline and fracture porosity (C) SEM backscatter image illustrating pore space geometry, and anhydrite cement effects. (D) Fine crystalline dolomite with intercrystalline and vuggy porosity, Bm-15, U2 (2580 m). (E) Coarse crystalline dolomite of Lithofacies 3 showing intercrystalline porosity Bm-15, U4 (2391 m). (F) SEM images showing pores shape and size in coarse crystalline dolomite, Bm-15, U4 (2391 m). (G) Fine crystalline dolomite of lithofacies 3 showing vuggy and fracture porosity, Bm-15, U4 (2450 m). (H) Coarse crystalline dolomite showing intercrystalline porosity and solution-enlarged vugs Bm-15, U4 (2391 m). (K) SEM images showing intercrystalline and vuggy porosity in medium dolomite crystals, Bm-15, U4 (2388m).

The separation between the neutron-density bulk porosity (ϕ_{nd}) and sonic porosity (ϕ_s) can be a good indicator of secondary porosity (Schlumberger, 1997) or of fractures in those units where there is no geochemical diagenesis apparent in the rocks. This study introduces the fracture-diagenesis indicator (FDI) as a term indicating both secondary porosity and fracturing has occurred. The FDI is the result of comparing the calculated SPI from the wireline logs and diagenesis and fracturing features that are characterised under the microscopic study. Calibration of the FDI was carried out by using a microscopic thin section study to identify whether the FDI was due to fracturing or other positive diageneses such as dissolution and dolomitisation (Figure 9).

Figure 9. Porosity distribution (bulk and effective) within the Butmah Formation at well Bm-15 with secondary porosity indicator (SPI) and fracturing-diagenesis indicator (FDI) at each depth.

6. DISCUSSION

This section considers three main issues; (i) integration of petrophysical properties with the qualitative description of controlling factors, (ii) using the integrated results to create a new method for calculating post- and pre-dolomitisation poroperm characteristics and its validation, (iii) identification the pore system and petrodiagenetic pathway of the Butmah Formation.

6.1 Integration of petrophysical properties and controlling factors

The porosity-permeability (poroperm) relationship in carbonate rocks is controlled by whether pores and vugs are inter-granular, inter-crystalline, separate or touching (Lucia, 2007). Each type has a different pore connectivity and size distribution. Hence, for the best interpretation, it is important to integrate the information of the pore space type in the facies with the poroperm relationship (Ma and Morrow, 1996; Tiab and Donaldson, 2012; Hommel et al., 2018; Bohnsack et al., 2020).

The position of each sample within the poroperm plot depends upon the degree of fracturing exhibited by the sample as well as the cementation exponent and grain size. In this study, we have spilt each of the limestone and dolomite poroperm relationships into three fields using the modified carbonate RGPZ poroperm relationship (Glover et al., 2006; Rashid et al., 2015b). This relationship can be expressed as

$$k = \frac{d_g^2}{4am^2\eta\phi^{-m}(\eta\phi^{-m}-1)^2} \approx \frac{d_g^2\phi^{3m}}{4am^2\eta^3} \; if \; \phi^{-1} \gg 1, \tag{1}$$

where k is permeability in (m^2), d_g is the characteristic grain size (in m), a=8/3, ϕ is the porosity (fractional), m is the cementation exponent (no units) and η is a factor expressing how the characteristic pore size of the rock is related to the characteristic grain size.

We have defined three fields within the poroperm relationship. Field D represents the poroperm characteristics of a rock which is controlled any degree of diagenesis without fracturing. Field F represents the poroperm characteristics of a rock which is controlled by fracturing with no appreciable diagenesis, while Field FD represents the poroperm characteristics of a rock partially controlled by diagenesis and partially by fracturing.

In Figure 10, the D/FD cut-offs are (η=1, m=2.0, d_g=1 μm) and (η=1, m=2.0, d_g=4 μm) for limestone and dolomite samples, respectively. For the FD/F boundary, the cut-off values are (η=1, m=1.8, d_g=10 μm) and (η=1, m=1.8, d_g=40 μm) for limestone and dolomite samples, respectively. The lower cementation exponent for the FD/F cut-off takes account for the lower cementation exponents associated with the decrease in pore space connectivities associated with fractures (Glover, 2015). For the D/FD cut-off, the characteristic grain sizes of 1 μm and 4 μm are associated with characteristic pore sizes of 0.002 μm and 0.0086 μm using the transformation given in Glover and Walker (2009) for a porosity of 5%. This transformation is given by

$$d_p^2 = \frac{8\phi^{2m}}{am^2} \cdot d_g^2 \,, \tag{2}$$

where all the parameters were defined for Eq. (1) except d_p, which is the pore diameter (same units as d_g). For the FD/F cut-off, the characteristic grain sizes of 10 μm and 40 μm are associated with characteristic pore sizes of 0.044 μm and 0.175 μm, also calculated from Equation (2) for a porosity of 5%, showing in all cases that the pore dimensions are significantly smaller than the grains that define them in both the limestones and the dolomites, but that the dolomite grains are significantly larger than those in the pre-dolomitised limestone, which is consistent with both our micrographical experience and those of others (Moore, 2001; Lucia, 2004; 2007).

In summary, the D field consists of samples whose petrophysical properties have developed mainly by diagenetic processes such as dolomitisation, dissolution, and cementation. The FD field consists of samples whose petrophysical properties have developed partially by fracturing and partially by diagenesis, and the F field contains the samples whose petrophysical properties have been improved mainly by fracturing, without or with minor diagenetic influence. Table 3 summarises the field and zone definitions that we have used, while Figure 10 shows all of the experimental data in the context of the defined fields and zones.

Table 3. The poroperm zones classification applied to the Butmah Formation

Lithology	Zone	Porosity (%)	Permeability (mD)	Pore throat (µm)	Controlling factor
Limestone	D	1.8 – 6.5	0.000001 - 0.001	0.001 – 0.1	Diagenesis
	FD	1.0 – 4.5	0.00001 – 0.02	0.08 – 1.0	Fracturing + diagenesis
	F	0.5 – 3.5	0.003 - 8.0	0.3 - 20	Fracturing
Dolomite	D	1.8 – 8.6	0.00005 - 0.05	0.02 – 1.0	Diagenesis
	FD	1.0 – 5.0	0.001 – 8.0	0.1 – 20	Fracturing + diagenesis
	F	1.5 - 2.5	0.8 - 8.0	8.0 - 18	Fracturing

D= diagenesis effect field, FD= fracturing and diagenesis effect field, F= fracturing effect field.

Figure 10. Porosity-permeability relationships with controlling factors shown as identified petrophysical fields. (A) The poroperm relationship for the limestone samples (U.5, L.1) with pie chart shows the distribution of the identified petrophysical fields. (B) The poroperm relationship for the dolomite samples (U.4, L.3) with pie chart shows the distribution of the identified petrophysical fields. The solid lines partitioning the poroperm relationships are RGPZ contours where the grain size (d) and cementation exponent (m) parameters are given in the figure (Glover et al., 2006; Rashid et al., 2015b). The dashed lines are best fit RGPZ-type power laws for each field.

Limestone Samples

The 43 limestone samples of the Butmah Formation have, in general, smaller porosity, pore throat and pore sizes and permeabilities than the dolomite samples. They can be divided into three fields, as follows.

D (Diagentically altered samples). This field consists of 32.6% of the limestone samples of the Butmah Formation and includes pore network consist of interparticles, intercrystalline, vugs and microfractures. Their permeability has been improved mainly by diagenetic processes, such as dissolution and cementation. These samples have porosity range between 1.8% and 6.5% and a permeability range between 1.0×10^{-6} mD and 1.0×10^{-3} mD, with a pore throat range between 0.001 µm and 0.1 µm. Figure 10A shows that these samples follow an RGPZ type power law (blue dashed line) with a power law coefficient of determination R^2=0.85, indicating that there is a small degree of heterogeneity. None of these samples showed any significant fracturing at microscopic or macroscopic scale.

FD (Fractured and diagenetically altered samples). This field represents 41.8% of the limestone samples of the Butmah Formation and contains samples which have a pore network consisting of interparticle and intercrystalline pores, together with microfractures. Their permeability has been improved both by fracturing and diagenetic processes such as dissolution and cementation. These samples have a porosity range between 1.0% and 4.5% and a permeability range between 10 nD and 0.02 mD with a pore throat range between 0.08 µm and 1.0 µm. The best-fit RGPZ-type power law that is shown by a dashed green line in Figure 10A shows that these samples are scattered, with a low power law coefficient of determination, R^2=0.57. This low value may be the result of the samples exhibiting a great deal of heterogeneity resulting from the porosity and permeability being affected by a large number of diagenetic processes and fracturing, the latter of which can amplify the degree of diagenesis locally.

F (Fractured samples). This field represents 25.6% of the limestone samples of the Butmah Formation. These samples have pore networks consisting of macroscopic fractures together with interparticle and intercrystalline pores, and microfractures. Their permeability has been improved predominantly by fracturing. These samples have porosity ranging between 0.5% and 3.5% and permeability ranging between 0.003 mD and 8.0 mD with 'pore throats' greater than 0.3 µm, which likely represent the apertures of fractures. The best-fit RGPZ-type power law that is shown by a dashed red line in Figure 10A shows that the fractured limestone samples are scattered, with a power law coefficient of determination R^2=0.25. The cause of the low coefficient of determination, here, is expected to be the presence of different degrees of fracturing in the data set, with the three lowest permeability points exhibiting only small degrees of fracturing.

Dolomite samples

A total of 47 samples of the dolomite lithology were analysed to calculate their petrophysical properties in the same way as for the limestone samples. These samples can also be divided into three fields.

D (Diagenetically altered samples). This field consists of 59.6% of the dolomite samples of the Butmah Formation and includes samples where the pore network consists of interparticle, intercrystalline, and vuggy pores, with some microfractures. Their permeability has been improved mainly by the diagenetic process of such as dissolution and cementation. These samples have a porosity range between 2.0% and 8.6%, permeability ranging between 5.0×10^{-5} mD and 5.0×10^{-2} mD, and pore throat diameters between 0.02 µm and 1.0 µm. The best-fit RGPZ-type power law, that is shown by a dashed blue line in Figure 10B, shows that these samples are scattered, with a power law coefficient of determination R^2=0.63, which is a larger degree of variation than that found for the Limestone Field D samples, described above, and indicates that is the dolomite exhibits a higher degree of heterogeneity than the limestone, which is caused by the development of a pore texture that is dependent on dolomitisation, dissolution and precipitation. None of these samples showed any significant fracturing at microscopic or macroscopic scale.

FD (Fractured and diagenetically altered samples). This field represents 31.9% of the dolomite samples of the Butmah Formation and has pore network consisting of both fractures (mainly microfractures) and interparticle or intercrystalline pores. Their permeability has been improved by both diagenesis and fracturing. The fracturing may have enhanced certain diagenetic processes, such as dissolution, compaction and cementation, by allowing the access and egress of fluids. Equally, the process of dolomitisation may have promoted the formation of fractures because dolomite is more brittle than limestones and would also be hosting a higher porosity matrix.

These samples have porosity range between 1.0% and 5.0%, a permeability range between 0.001 mD and 8.0 mD, and have pore throat diameters between 0.1 µm and 20 µm. The best-fit RGPZ-type power law that is shown by a dashed green line in Figure 10B shows that these samples show a high degree of variation, with a power law coefficient of determination R^2=0.49. This value slightly lower than the Limestone FD samples, which may be due to the process of dolomitisation largely reworking the pore texture, making it more locally heterogeneous.

F (Fractured samples). This field represents 8.5% of the dolomite samples of the Butmah Formation. These samples have a pore network that consists of some interparticle and intercrystalline pores, but that is dominated by macroscopic fractures and microfractures. As a result, their permeability has been enhanced mainly by fracturing. These samples have porosity range between 1.5% and 2.5%, permeabilities between 0.8 mD and 8.0 mD, with pore throat diameters greater than 8.0 µm. As for fractured limestones, the largest pore diameters are probably measurements of the apertures of fractures. In Figure 10B the best-fit RGPZ-type power law (shown by a dashed red line) is almost meaningless because it is based on only 4 datapoints. However, it gives a power law coefficient of determination R^2=0.42, which is consistent with an RGPZ trend. This is mainly due to the fact that locally some samples were substantially fractured while others were only slightly fractured, in a small sample set where variability can be significantly changed by one unusual sample.

6.2 New method for calculating post- and pre-dolomitisation poroperm characteristics

Relative poroperm characteristics

Comparison between the difference in the petrophysical properties of each lithology (limestone and dolomite) samples of the Butmah Formation is very important for three reasons. First, in order to ascertain the petrodiagenetic pathway of carbonate rocks (Mohammed Sajed and Glover, 2020). Second, to obtain the pre-dolomitisation petrophysical properties of dolomite samples, and thirdly, to predict the post-dolomitisation petrophysical properties of limestone samples. Accordingly, a non-linear best fitting process was carried out on each of the 6 fields. In all cases the best fitting equation was a power law, and these are given in Table 4 and Figure 11. It was expected that a power law would represent the best-fitting equation because the generic RGPZ model (Glover et al., 2006; Rashid et al., 2015b) has a power law form which arises from its theoretical pedigree. Hence the fit is informed by the physics of the porous medium to which it is being applied. It follows that the RGPZ equations, when written in the generic power law form provide good fits with high values of coefficient of determination (R^2) compared to all other *ad hoc* fitting types (Rashid et al., 2015b; Al-Khalifah et al., 2020).

It should be noted that these equations were identified for the Butmah Formation, and any other carbonate formation needs to find its own best-fit equations. However, since the RGPZ equations present a generic form of the fitting equations and were ultimately derived theoretically rather than simply being empirical fits (Glover et al., 2006), it is more than likely that the best fitting will commonly be attained by using a power law fit.

Figure 11 shows a comparison of the poroperm trends for each of the three identified fields. Figure 11A shows that the diagenetically-altered limestone samples increase in permeability as porosity increases with a power law coefficient of determination R^2=0.85. The increase in porosity is related mainly to dissolution and increases at a rate dependent upon the connectivity of the pores. By contrast, the diagenetic dolomite samples in Figure 11A show a similar increase in permeability with porosity (R^2=0.63) but to higher porosities and permeabilities that are due to dissolution and dolomitisation. The difference in the porosity ranges of the limestone and dolomite samples is approximately 1.5 units. Whereas Figure 11B shows only one unit different between the porosity range of limestone and dolomite samples, with a low power law coefficient of determination (R^2=0.49 and 0.57 respectively) as a result of the effect of diagenesis and fracturing controls. The dolomite samples were more heterogeneous due to effect of dolomitisation compared to the limestone samples.

Table 4. Permeability estimating equations for the 3 identified fields for each limestone and the dolomite samples.

Lithology	Field	Equation (k *in mD and* ϕ *as a percentage*)	Limits of validity
Limestone	D	$k_D = 2\times10^{-8}\phi^{5.2579}$	Porosity: 1.8% - 6.5% Permeability: 10^{-6} – 10^{-3} mD Pore throat diameter: 0.001 – 0.1 μm Grain diameter: < 1 μm Cementation exponent: > 2
	FD	$k_{FD} = 2\times10^{-5}\phi^{3.9099}$	Porosity: 1.0% - 4.5% Permeability: 10^{-5} – 2×10^{-2} mD Pore throat diameter: 0.08 – 1.0 μm Grain diameter: 1 - 10 μm Cementation exponent: 1.8 - 2
	F	$k_F = 4\times10^{-2}\phi^{3.4569}$	Porosity: 0.5% - 3.5% Permeability: 0.003 – 8.0 mD Pore throat diameter: 0.3 – 20 μm Grain diameter: > 10 μm Cementation exponent: < 1.8
Dolomite	D	$k_D = 3\times10^{-6}\phi^{3.7444}$	Porosity: 1.8% - 8.6% Permeability: 5×10^{-5} – 5×10^{-2} mD Pore throat diameter:0.02 – 1.0 μm Crystal diameter: < 4 μm Cementation exponent: > 2
	FD	$k_{FD} = 1.1\times10^{-3}\phi^{4.3692}$	Porosity: 1.0% - 5.0% Permeability: 10^{-3} – 8.0 mD

		Pore throat diameter: 0.1 – 20 μm Crystal diameter: 4 - 40 μm Cementation exponent: 1.8 - 2
F	$k_F = 0.5877\phi^{1.7574}$	Porosity: 1.5% - 2.5% Permeability: 0.8 – 8.0 mD Pore throat diameter: 8.0 – 18 μm Crystal diameter: > 1 μm Cementation exponent: < 1.8

Figure 11. Comparison of the three identified petrophysical fields in both lithology limestone and dolomite including porosity, permeability, and the non-linear best fitting equations with a power law coefficient of determination (R^2). (A) Diagenetically altered samples. (B) Fractured and diagenetically- altered samples. (C) Fractured samples.

Figure 11C shows that there is complete overlap between the fractured limestone and dolomite due to the degree of scatter in both datasets, with a low power law coefficient of determination (R^2=0.25 and 0.42 respectively). This is mainly due to the fact that some samples were substantially fractured while others were only slightly fractured. This may be a result of the measurements being made on core samples, which are sufficiently small for the full expression of fracturing not to be taken into account in the data. Indeed, it is likely that only the higher permeability group in Figure 11C are truly caused by fracturing, while some of the smaller permeability values, though high for their individual porosity, are due to relict diagenetic processes, particularly dissolution. This same separation of the fractured samples is shown to a lesser degree for the fractured dolomite samples, probably for the same reason.

Predicting pre- and post-dolomitisation porosity

This study applies a new method for

(i) estimating the petrophysical properties of dolomite if the petrophysical properties of the pre-dolomitised limestone are known, or

(ii) estimating the petrophysical properties of the pre-dolomitised limestone from knowledge of the petrophysical properties of the existing dolomite.

The methodology takes account of varying porosity values and uses a non-linear best fitting process to ensure that transformation of data for individual samples is carried out with contributing canonical averages for the whole related dataset. Calculations were carried out on each of the 6 fields (limestone to dolomite and vice versa, for D, FD and F data).

For the process of dolomitisation (i.e., calcite becoming dolomite mineral) the methodology uses the following steps, the results of which are shown in figures 12 to 14 for each of the D, FD and F data, respectively.

1- Plot the samples on the poroperm plot (e.g., Figure 12A).
2- Apply the power law fitting equation to the limestone samples (e.g., Figure 12A).
3- Using a millimetric scale to measure the high and low of plotting sample of the best fitting line (e.g., Figure 12A).
4- Calculate the difference in the porosity ranges between the limestone and dolomite samples using Equation (3) for each identified (D, FD and F) as follows;

$$\psi_f = \frac{(\phi_{dol\_hi} - \phi_{dol\_low})}{(\phi_{lmst\_hi} - \phi_{lmst\_low})}, \quad (3)$$

where ψ_f is the fractional relative variation of the dolomite samples with respect to the variation in the limestone samples in a particular field (*f*), whether D, FD or F. The other parameters in Equation (3) are ϕ_{dol_hi}, which is the highest calculated porosity in the dolomite samples, ϕ_{dol_low}, which is the lowest calculated porosity in the dolomite samples, ϕ_{lmst_hi}, which is the highest calculated porosity in the limestone samples, and ϕ_{lmst_low}, which is the lowest calculated porosity in the limestone samples.

In this study, ψ_f was found to be 1.49 for diagenetically-altered samples, 1.05 for fractured and diagenetically-altered samples, and 0.51 for fractured samples.

5- Add the porosity percentage to each limestone sample.
6- Replot the new porosities together with the permeability calculated by applying the non-linear best fitting equation for the dolomite samples on a poroperm plot (e.g., Figure 12B). At this stage all the predicted points fall exactly on the fitting curve. The next step restores the scatter to the data points.

7- Use the millimetric scale again to give the high and low of each sample according to the earlier measurements in Point 3 in this list to give the best estimated values of post-dolomitisation limestone samples including scatter (e.g., Figure 12C).

8- Plot the origin limestone measurements with the post-dolomitisation limestone samples to compare the result (e.g., Figure 12D).

It is important to note that the millimetric scale represents an arbitrary scale that measures the scatter in data points and is valid irrespective of the other relative scales and units if applied consistently. The calculation of ψ_f is consequently non-dimensional.

We can also apply the same processes 'in reverse' to estimate the petrophysical properties of pre-dolomitisation limestone from the dolomite samples of the Butmah Formation (e.g., Figure 12E-H).

Figures 13 and 14 show the same procedure that has been applied in Figure 12, but for samples that are altered both by fracturing and diagenesis (Figure 13), and for samples that are only altered by fracturing (Figure 14).

Figure 12. Prediction of post-dolomitisation dolomite poroperm data and the pre-dolomitisation limestone data for the diagenetically-altered samples (Field D). (A-D) The limestone samples (U.5, L.1) are used to estimate their post-dolomitisation petrophysical properties. (E-H) The dolomite samples (U.4, L.3) are used to estimate the pre-dolomitisation petrophysical properties.

Figure 13. Prediction of post-dolomitisation dolomite poroperm data and the pre-dolomitisation limestone data for the fractured and diagenetically altered samples. (A-D) The limestone samples (U.5, L.1) are processes of estimating the post-dolomitisation petrophysical properties. (E-H) The dolomite samples (U.4, L.3) are processes of the pre-dolomitisation petrophysical properties.

Figure 14. Prediction of post-dolomitisation dolomite poroperm data and the pre-dolomitisation limestone data for the fractured samples. (A-D) The limestone samples (U.5, L.1) are processes of estimating the post-dolomitisation petrophysical properties of limestone samples. (E-H) The dolomite samples (U.4, L.3) are processes of the pre-dolomitisation petrophysical properties.

Figure 15 shows comparisons between the predicted and the measured values for the post-dolomitisation and pre-dolomitisation values. There is good correspondence in all the comparisons. However, the weakest correspondence occurs for the F field, where the small number of samples has made the method more inaccurate.

Table 5 summarises the results of carrying out two sample *t*-tests on the data, which is required in order to quantify the extent to which the new method is effective. Two sample *t*-tests have the capability of distinguishing whether the two samples, here predicted and associated measured values, are different, that is, they are not drawn from the same population and cannot be considered to be statistically equal within a given probability. In our case we are looking for statistical evidence that the opposite is the case. In other words, that the predicted and measured data seem to be drawn from the same population and hence are identical.

In our case we do this for both the porosity and the permeability separately, using Welch's unequal variances *t*-test formulation (Delacre et al., 2017). This formulation takes account of unequal variances in the two sample sets. All of the requirements of using this test are fulfilled. That is to say that (i) the data consists of two independent samples, one from each of the two populations being compared (here the measured and predicted data), (ii) the sample means are normally distributed, (iii) the sample variances are $\chi 2$ distributed, which follows from (ii), and (iv) the sample means and sample variances are statistically independent. We have pre-tested for normality for all of our porosity data using the Kolmogorov-Smirnov test. All porosity data was found to be distributed normally. However, permeability is commonly distributed log-normally, and is so in our datasets. Consequently, we have carried out all statistical tests on the logarithm to the base 10 of permeability data. When this logged data was subjected to the Kolmogorov-Smirnov test, normality was found in all cases.

We have calculated a *t*-statistic, a critical *t*-value and a *P*-value using the Welch's unequal variances *t*-test formulation (Delacre et al., 2017) and taking account of the variable degrees of freedom between the D, DF and F field data, and these are shown in Table 5.

The criteria that that the predicted and measured data are drawn from the same population and hence are identical is that the *t*-value is as close to zero as possible, and that the *t*-value is less than, preferably much less than the *t*-critical value. This is clearly the case for all of the D and DF field data shown in the table. The evidence is weaker for the F field data because there are only 4 samples in the dolomite F dataset, which weakens the statistical power of the calculation. Consequently, on the basis of the *t*-test, it might be said that the predicted permeabilities agree well with the associated experimental data. Hence the new method works well, at least for the D and the DF data, and might work well for the F data if we had a sufficiently large dataset to test it more thoroughly.

We have also calculated the *P*-value from the *t*-value statistic. Since we are seeking the fulfilment of the null hypothesis rather than when it fails, this statistic is difficult to interpret. The *P*-value is normally used to recognise the probability that the null hypothesis (here that the two datasets have equal mean values, i.e., H_o: $\mu_1=\mu_2$) is apparently broken by chance. For example, two very different, but maybe slightly overlapping datasets might have a *P*-value of 0.02, representing a 2% chance that the data seem to be separated but are in fact from the same population. In this work we obtain values as high as 0.863 indicating that it is highly likely that the data are from the same population – 86.3% chance in fact.

Table 5. Statistical 2 sample *t*-tests on the data using Welch's unequal variances *t*-test (Delacre et al., 2017) with a level of probability of 95% (0.05). Permeability data have been calculated on the base 10 logarithm of the data value to take account of the log-normal distribution of the permeability data. All porosity data and $\log_{10}$(permeability) data passed the Kolmogorov-Smirnov test for normality.

Field	Prediction	Variable	Dataset	Sample size	Mean (%)	Standard deviation (%)	*t*-statistic		*t*-critical at α=0.05	*P*-value
D	Post-dolomitisation	Porosity	Predicted	14	5.343	1.364	0.322	<<	2.032	0.749
			Measured	28	5.178	1.921				
D	Post-dolomitisation	$\log_{10}$(Permeability)	Predicted	14	-2.797	0.576	0.54	<<	2.028	0.592
			Measured	28	-2.919	0.870				
D	Pre-dolomitisation	Porosity	Predicted	28	3.687	1.921	0.322	<<	2.030	0.749
			Measured	14	3.854	1.364				
D	Pre-dolomitisation	$\log_{10}$(Permeability)	Predicted	28	-4.573	1.514	0.876	<<	2.026	0.386
			Measured	14	-4.237	0.953				
DF	Post-dolomitisation	Porosity	Predicted	18	3.520	1.043	0.292	<<	2.048	0.772
			Measured	15	3.407	1.170				
DF	Post-dolomitisation	$\log_{10}$(Permeability)	Predicted	18	-0.697	0.914	0.174	<<	2.048	0.863
			Measured	15	-0.757	1.047				
DF	Pre-dolomitisation	Porosity	Predicted	15	2.357	1.170	0.292	<<	2.048	0.772
			Measured	18	2.471	1.043				
DF	Pre-dolomitisation	$\log_{10}$(Permeability)	Predicted	15	-3.467	1.647	0.245	<<	2.074	0.808
			Measured	18	-3.346	1.043				
F	Post-dolomitisation	Porosity	Predicted	11	2.440	0.736	1.466	<	2.306	0.166
			Measured	4	1.950	0.500				
F	Post-dolomitisation	$\log_{10}$(Permeability)	Predicted	11	0.506	0.902	0.785	<	2.179	0.447
			Measured	4	0.258	0.324				
F	Pre-dolomitisation	Porosity	Predicted	4	1.440	0.500	1.466	<	2.306	0.166
			Measured	11	1.930	0.736				
F	Pre-dolomitisation	$\log_{10}$(Permeability)	Predicted	4	-0.891	0.642	0.851	<	2.262	0.41
			Measured	11	-0.502	1.079				

We hypothesize that we do not have *P*-values higher than 0.863, and approaching unity, because we are constrained to testing the predicted porosity and permeability after dolomitisation with the actual measured porosity and permeability after dolomitisation on closely associated units. The diversion from unity represents the natural variability between the petrophysical properties of the predicted rock from the nearby test rock, which may be different. The same effect also occurs when predicting porosity and permeability before dolomitisation. Consequently, it might be expected that a value closer to unity than 0.863 would not be expected, indeed that values between 0.7 and 0.9 are very creditable. If this is the case, for a *P*-value of 0.863, the value 0.137 (=1-0.863) represents some measure of the variability between the rock used for prediction and the test rock. Nonetheless, we also obtain a few lower values for the permeability predictions in the Field D as well as lower values still for the statistically weak tests carried out for Field F.

In summary, both Figure 15 and Table 5 provide strong quantitative evidence for a good correlation in most of the 16 tests. This data leads us to believe that the new method represents a useful new approach to predicting the porosity and permeability of limestone rocks post-dolomitisation, and obtaining the likely porosity and permeability of dolomitised rocks before the dolomitisation occurred. Here, this new method was applied to the Butmah Formation as an example that could be easily applied to any other carbonate formations using the same processes to cover any shortage of core samples in some formation intervals within boreholes and to obtain an integrated reservoir characterisation.

Figure 15. Comparison of the modelled post-dolomitisation and pre-dolomitisation porosity and measured permeability values with values from associated dolomite and limestones, respectively. (A) predicted and measured values for post-dolomitisation dolomite in diagenetic field samples (Field D), (B) predicted and measured values for pre-dolomitisation limestone in diagenetic field samples (Field D), (C) predicted and measured values for post-dolomitisation dolomite in fractured-diagenetic field samples (Field FD), (D) predicted and measured values for pre-dolomitisation limestone in fractured-diagenetic field samples (Field FD), (E) predicted and measured values for post-dolomitisation dolomite in fractured field samples (Field F), (F) predicted and measured values for pre-dolomitisation limestone in fractured field samples (Field F).

6.3 The pore system and petrodiagenetic pathway of the Butmah Formation

The qualitative observations of the diagenesis in the Butmah Formation were characterised by three stages (Figure 4); a syndepositional and marine diagenetic stage (Stage-1), a meteoric and mixing zone diagenetic stage (Stage-2), and a burial diagenetic stage (Stage-3).

The major dolomitisation phase of the Butmah Formation is either syndepositional or occurs during shallow-burial conditions associated with anhydrite cement and ends before significant burial occurs (Mohammed Sajed and Glover, 2022). Accordingly, early dolomitisation plays a significant role in improving the reservoir properties of the Butamh Formation in Stage-1. Whereas, intergranular/intercrystal, solution-enlarged vugs and selective dissolution were the main factors improving the reservoir properties in Stage-2, the main factor in Stage 3 was fracturing. Stage-3 processes have affected all the stratigraphic units of the Butmah Formation in two ways. First, reduction in matrix porosity by dolomite recrystallization, cementation, and significant compaction. Second, increased fracture intensity due to high compaction (chemical compaction) (Mohammed Sajed and Glover, 2020).

Consequently, the final shape of the pore network of the Butmah Formation was described in stratigraphic units 1, 3, and 5 as pores are mainly due to a combination of dissolution, cementation, and fracturing controls, whereas stratigraphic units 2 and 4 are more complicated by including dolomitisation to dissolution, cementation, and fracturing controls.

In general, porosity in carbonate rocks is secondary porosity caused mainly by dissolution, dolomitisation and fracturing (Ahr, 2008; Mohammed Sajed and Glover, 2020; Quan et al., 2023). The separation between the bulk porosity (ϕ_{nd}) and sonic porosity (ϕ_s) can be a good indicator of secondary porosity (Schlumberger, 1997) or of fractures in those units where there is no geochemical diagenesis apparent in the rocks and it is often used to indicate the extent of diagenetic reworking of porosity (Wyllie et al., 1956, 1958; Asquith and Gibson, 1982; Bateman, 1985; Schlumberger, 1989). Accordingly, this study used the fracture-diagenesis indicator (FDI) for comparing the calculated SPI from the wireline logs and diagenesis and fracturing features that are characterised under the microscopic study to identify whether the FDI was due to fracturing (F) field or other positive diageneses such as dissolution and dolomitisation (D) field or mixture of both (FD) field (Figure 9). Only U.1 shows the effect of the three controlling factors D, DF, and F whereas, U.2 and U.4 were influenced by D and FD and U.3 and U.5 were affected by FD and F.

The quantitative observations of the Butmah Formation including porosity, permeability and pore throat measurements were integrated with the qualitative description of the diagenetic and fracturing controls allowed us to split the poroperm relationship of the Butmah Formation using the modified carbonate RGPZ poroperm relationship (Glover et al, 2006; Rashid et al., 2015b) into three petrophysical fields for each limestone and dolomite lithology according to their grain/crystal size, and cementation exponent that take account of whether the main control on petrophysical properties and reservoir quality is diagenesis (D), fracturing (F) of a mixture of both (FD) to illustrate clearly that the general pore system in the Butmah Formation can be described as a hybrid, diagenetic-fracturing pore system according to Ahr's classification (2008), with 32.6% diagenetic petrophysical field, 41.8% fracturing-diagenetic petrophysical field and 25.6% fracturing petrophysical field for limestone. Whereas for the dolomite the diagenetic petrophysical field represented by 59.6% and 31.9% and 8.5% for the diagenetic, fracturing-diagenetic, and fracturing petrophysical fields respectively.

Diagenesis and fracturing can cause increases or decreases in both porosity and permeability, fracturing generally results in smaller changes to porosity and larger changes to permeability than diagenetic processes. Consequently, diagenesis and fracturing can work together to make the pore network of carbonate reservoirs more heterogeneous resulting in a hybrid porosity system (Tuker et al., 1990; Selly, 2000; Scholle and Ulmer Scholle, 2003; Ahr, 2008; Boggs, 2009; Ross, 2011; Mohammed-Sajed and Glover, 2022). The Butmah Formation shows this tendency well, with fractured samples plotting on the poroperm plots at high permeabilities and low porosities (Field F), whereas diagenetically-altered samples show moderately high permeabilities but substantially higher porosities (Field D) (Figure 10).

Consequently, the integrated result of applying the qualitative description and the quantitative measurements and predictions presented in this study, the main petrodiagenetic pathways of the Butmah Formation according to the effect of dolomitisation and fracturing can be summarised in Figure 16. This figure illustrates that dolomitisation generally increases porosity and permeability even if the rocks are previously fractured. The effect of dolomitisation alone on the limestone samples shows notable changes in porosity and permeability (Figure 16A). The dolomitisation effect on the partially fractured limestone samples also shows a notable increase in both permeability and porosity, (16B). The dolomitisation effect on the fully fractured limestone samples shows an increase in permeability but no apparent increase or decrease in porosity (Figure 16C). This may be due to the small numbers of samples in the fractured set.

Fracturing occurring in either a limestone or a dolomite with no further dolomitisation (Figure 16D and 16E, respectively, provided significant increases in permeability despite also showing decreases in porosity. This is contrary to expectations, and it is thought that some other diagenetic process, such as matrix precipitation, is also contributing to the changes in the petrodiagenetic pathway. It is worth noting that the decrease in porosity on fracturing is larger if it happens to dolomitised rock (Figure 16E).

Figure 16. The petrodiagenetic pathway of the Butmah Formation according to the effect of dolomitisation and fracturing. (A) Dolomitisation of limestone. (B) Dolomitisation of partially fractured limestone. (C) Dolomitisation of fully fractured limestone. (D) Fracturing of limestone with no dolomitisation. (E) Fracturing of dolomite.

Moreover, Figure 17 summarises in an overall flow diagram, the qualitative and quantitative observations and inferences set out in this paper from two points of view; (i) qualitative descriptions including diagenetic stages, main controlling factors and pore types and their outcome as pore network and pore system, and (ii) quantitative descriptions and measurements, including field-based poroperm classifications as a new technique and their outcome to divided it into petrophysical fields according to the characterised main controlling factors (fracturing and diagenetic), and the changes in the petrophysical properties including porosity, permeability and pore throat size.

Figure 17. Flow chart summarising the qualitative and quantitative descriptions of the petrodiagenetic pathway of the Butmah Formation (ϕ, porosity; k, permeability; d_{th}, characteristic pore throat diameter.

7. CONCLUSIONS

The results of this study may be summed up as follows;

- The Butmah Formation has been affected by several diagenetic processes characterised by three diagenetic stages that create the final pore system of the Butmah Formation, which are; a syndepositional and marine diagenetic stage, a meteoric and mixing zone diagenetic stage, and a burial diagenetic stage. Consequently, the final shape of the pore network described in units 1, 3, and 5 as pores are mainly due to a combination of dissolution, cementation, and fracturing controls, whereas units 2 and 4 are more complicated by adding dolomitisation to dissolution, cementation, and fracturing controls.
- Three petrophysical fields have been identified according to their poroperm relationships that take account of whether the main control on petrophysical properties and reservoir quality is diagenesis, fracturing, or a mixture of both.
- A new method of estimation the petrophysical properties of limestones if they are subjected to dolomitisation and of dolomites before they were dolomitised has been developed. The method relies on the fitting of some theoretical non-linear equations to the identified petrophysical fields and controlling scatter. The new method has been validated against associated data from the Butmah Formation and found to work well. This new method can be applied easily to any other carbonate formations using the same processes to cover any shortage of core samples in some formation intervals within boreholes and to obtain an integrated reservoir characterisation.
- While this work has defined no explicit consecutive petrodiagenetic pathway for the Butmah Formation, it has helped define the size and direction of five individual diagenetic

and fracturing events that are the building blocks of such a pathway. These events are (i) dolomitisation, (ii) dolomitisation of partially fractured rocks, (iii) dolomitisation of fully fractured rocks, (iv) fracturing with no dolomitisation, and (v) fracturing from dolomitized rocks.

ACKNOWLEDGEMENTS

The authors are grateful to the Iraqi North Oil Company for providing the study's core samples and data, and Dr. Samuel Allshorn of the Wolfson Laboratory where many of the measurements were carried out.

REFERENCES

Adelinet, M., Barthélémy, J.F., Bemer, E. and Hamon, Y., 2019. Effective medium modeling of diagenesis impact on the petroacoustic properties of carbonate rocks. Geophysics, 84(4), pp.WA43-WA57.

Agar, S. M., and Geiger, S., 2014. Fundamental controls on fluid flow in carbonates: current workflows to emerging technologies. The Geological Society of London, special publications, v. 406, p. 1-59.

Ahr, W.M., 2008. Geology of carbonate reservoirs: the identification, description, and characterization of hydrocarbon reservoirs in carbonate rocks. Canada, John Wiley & Sons, Inc., Hoboken, New Jersey, 296 p.

Aleali, M., Rahimpour-Bonab, H., Moussavi-Harami, R., & Jahani, D. 2013. Environmental and sequence stratigraphic implications of anhydrite textures: A case from the Lower Triassic of the Central Persian Gulf. Journal of Asian Earth Sciences, 75, p.110-125.

Al-Khalifah, H., Glover, P.W.J. and Lorinczi, P., 2020. Permeability prediction and diagenesis in tight carbonates using machine learning techniques. Marine and Petroleum Geology, 112.

Alsharhan, A.S. 2006. Sedimentological character and hydrocarbon parameters of the middle Permian to Early Triassic Khuff Formation, United Arab Emirates. GeoArabia, 11, 121–158.

Amel, H., Jafarian, A., Husinec, A., Koeshidayatullah, A., Swennen, R., 2015. Microfacies, depositional environment and diagenetic evolution controls on the reservoir quality of the Permian Upper Dalan Formation, Kish Gas Field, Zagros Basin, Marine and petroleum geology, 67, 57-71.

Anselmetti, F.S., Eberli, G.P., 1993. Controls on sonic velocity in carbonates. Pure and Applied Geophysics, 141, p. 287-323.

Aqrawi, A. A. M., Goff, J. C., Horbury, A. D., and Sadooni, F. N., 2010. The petroleum geology of Iraq. Scientific Press Ltd, Beaconsfield, Bucks, 424 p.

Arosi, H.A. and Wilson, M.E., 2015. Diagenesis and fracturing of a large-scale, syntectonic carbonate platform. Sedimentary geology, 326, pp.109-134.

Asquith, G.B. and Gibson, C.R., 1982. Basic well log analysis for geologists, American Association of Petroleum Geologists, Tulsa, Oklahoma, 216 p.

Asquith, G., and Krygowski, D., 2004. Basic well log analysis. American Association of Petroleum Geologists, Tulsa, Oklahoma, 244 p.

Baqués, V., Ukar, E., Laubach, S.E., Forstner, S.R. and Fall, A., 2020. Fracture, dissolution, and cementation events in ordovician carbonate reservoirs, Tarim Basin, NW China. Geofluids, 2020.

Bateman R. M., 1985. Open-hole log analysis and formation evaluation. International Human Resources Development Corperation, Boston, p 647.

Bellen, R. C. V., Dunnington, H., Wetzel, R. and Morton, D., 1959. Lexique stratigraphique. International, Asie, Iraq, 333 p.

Boggs Jr, S., 2006. Sedimentology and stratigraphy. 4th edition, Pearson Education, 662p.

Boggs Jr, S., 2009. Petrology of Sedimentary Rocks. 2nd edition, Cambridge University Press, New York, 600p.

Bohnsack, D., Potten, M., Pfrang, D., Wolpert, P. and Zosseder, K., 2020. Porosity–permeability relationship derived from Upper Jurassic carbonate rock cores to assess the regional hydraulic matrix properties of the Malm reservoir in the South German Molasse Basin. Geothermal Energy, 8, p.1-47.

Bourque, P.A., Savard, M.M., Chi, G. and Dansereau, P., 2001. Diagenesis and porosity evolution of the upper silurian-lowermost devonian west point reef limestone, eastern Gaspe Belt, Quebec Appalachians. Bulletin of Canadian Petroleum Geology, 49(2), p.299-326.

Brigaud, B., Vincent, B., Durlet, C., Deconinck, J.F., Blanc, P. and Trouiller, A., 2010. Acoustic properties of ancient shallow-marine carbonates: effects of depositional environments and diagenetic processes (Middle Jurassic, Paris Basin, France). Journal of Sedimentary Research, 80(9), p.791-807.

Caine, J.S., Evans, J.P. and Forster, C.B., 1996. Fault zone architecture and permeability structure. Geology, 24(11), pp.1025-1028.

Cerepi, A., Barde, J.P. and Labat, N., 2003. High-resolution characterization and integrated study of a reservoir formation: the danian carbonate platform in the Aquitaine Basin (France). Marine and petroleum geology, 20 (10), p.1161-1183.

Childs, C., Walsh, J.J., Watterson, J., 1997. Complexity in fault zone structure and implications for fault seal prediction. In: Møller-Pedersen, P., Koestler, A.G. (Eds.), Hydrocarbon Seals: Importance for Exploration and Production. (Elsevier) Norwegian Petroleum Society Special Publication, 7, p. 61–72.

Choquette, P. W., and Pray, L. C., 1970. Geological Nomenclature and classification of porosity in sedimentary carbonates. American Association of Petroleum Geologists Bulletin, 54, p. 819-834.

Corrêa, R.S., Ukar, E., Laubach, S.E., Aubert, I., Lamarche, J., Wang, Q., Stockli, D.F., Stockli, L.D. and Larson, T.E., 2022. Episodic reactivation of carbonate fault zones with implications for permeability–An example from Provence, Southeast France. Marine and Petroleum Geology, 145, p.105905.

Delacre, M., Lakens, D., & Leys, C., 2017. Why Psychologists Should by Default Use Welch's t-test Instead of Student's t-test. International Review of Social Psychology, 30(1). https://doi.org/10.5334/irsp.82.

de Lima, A., Lopes, J.A., Medeiros, W.E., Schiozer, D.J., La Bruna, V. and Bezerra, F.H., 2023. Impact of fracture set scales and aperture enlargement due to karstic dissolution on the fluid flow behavior of carbonate reservoirs: A workflow to include sub-seismic fractures in 3D simulation models. Geoenergy Science and Engineering, 221, p.211374.

Dickson, J. A. D., 1965. A modified staining technique for carbonates in thin section: Nature, 205, p.587-587.

Dunnington, H. V., 1958. Generation, Migration, Accumulation and Dissipation of Oil in Northern Iraq: Middle East, American Association of Petroleum Geologists, special volume, p. 1194-1251.

Ehrenberg, S.N., 2004. Factors controlling porosity in Upper Carboniferous– Lower Permian carbonate strata of the Barents Sea. AAPG bulletin, 88 (12), pp.1653-1676.

Ehrenberg, S.N., Nadeau, P.H. and Aqrawi, A.A.M., 2007. A comparison of Khuff and Arab reservoir potential throughout the Middle East. AAPG bulletin, 91(3), pp.275-286.

Erdman, N. and Bell, D.C., 2015. Scanning Electron and Ion Microscopy of Nanostructures. In Nanocharacterisation, Royal Society of Chemistry, p. 300-350.

Esrafili-Dizaji, B. and Rahimpour-Bonab, H., 2009. Effects of depositional and diagenetic characteristics on carbonate reservoir quality: a case study from the South Pars gas field in the Persian Gulf. Petroleum Geoscience, 15 (4), p.325344.

Flugel, E., 2010. Microfacies of carbonate rocks. Verlag Berlin Heidelberg, 984 p.

Forstner, S.R. and Laubach, S.E., 2022. Scale-dependent fracture networks. *Journal of Structural Geology*, *165*, p.104748.

Fouad, S. F. A., 2015. Tectonic map of Iraq, scale 1: 1000 000, 3rd edition, Iraqi Bulletin of Geology and Mining, Papers of the Scientific Geological Conference, 11, p. 1-7.

Géraud, Y., Diraison, M. and Orellana, N., 2006. Fault zone geometry of a mature active normal fault: a potential high permeability channel (Pirgaki fault, Corinth rift, Greece). Tectonophysics, 426 (1), p.61-76.

Giesche, H., 2006. Mercury porosimetry: a general (practical) overview. Particle & particle systems characterization, 23(1), p.9-19.

Glover, P.W.J., Zadjali, I.I., Frew, K.A., 2006. Permeability prediction from MICP and NMR data using an electrokinetic approach. Geophysics, 71 (4), p.49-60.

Glover, P.W.J. and Walker, E., 2009. Grain-size to effective pore-size transformation derived from electrokinetic theory. Geophysics, 74(1), pp. E17-E29.

Glover, P.W.J. and Déry, N., 2010. Streaming potential coupling coefficient of quartz glass bead packs: Dependence on grain diameter, pore size, and pore throat radius. Geophysics, 75(6), p. F225-F241.

Glover, P.W.J., 2015. Geophysical Properties of the Near Surface Earth: Electrical Properties. Treatise on Geophysics: Second Edition. pp. 89-137.

Glover, P.W.J., Mohammed-Sajed, O.K, Cenk Akyüz, C., Lorinczi, P. and Collier, R. E. Ll., 2022, Clustering of facies in tight carbonates using machine learning, Marine and Petroleum Geology, published online 105828. 10.1016/j.marpetgeo.2022.105828

Gluyas, J. and R. Swarbrick, 2004. Petroleum Geoscience. Blackwell Science Ltd, 349p.

Hart, E. and J.T.C. Hay, 1974, Structure of Ain Zalah Field, Northern Iraq. AAPG Bulletin, 58(6), p.973-981.

Haines T.J., Michie, E.A.H., Neilson, J.E., and Healy, D. 2016. Permeability evolution across carbonate hosted normal fault zones, Marine and Petroleum Geology, 72, p. 62-82.

Hollis, C., Vahrenkamp, V., Tull, S., Mookerjee, A., Taberner, C. and Huang, Y., 2010. Pore system characterisation in heterogeneous carbonates: An alternative approach to widely-used rock-typing methodologies. Marine and Petroleum Geology, 27(4), pp.772-793.

Hollis, C., 2011. Diagenetic controls on the reservoir properties of carbonate successions within the Albian-Turonian of the Arabian plate. Petroleum Geoscience, 17, p. 223-241.

Hommel, J., Coltman, E. and Class, H., 2018. Porosity–permeability relations for evolving pore space: a review with a focus on (bio-) geochemically altered porous media. Transport in Porous Media, 124(2), pp.589-629.

Jannot, Y., Lasseux, D., Vizé, G. & Hamon, G. 2007. A detailed analysis of permeability and Klinkenberg coefficient estimation from unsteady-state pulsedecay or draw-down experiments. Paper No. SCA2007-08.

Jennings, J.B., 1987. Capillary pressure techniques: application to exploration and development geology. AAPG Bulletin, 71(10), p.1196-1209.

Jiang, L., Worden, R.H., Cai, C.F., Shen, A. and Crowley, S.F., 2018. Diagenesis of an evaporite-related carbonate reservoir in deeply buried Cambrian strata, Tarim Basin, Northwest China. AAPG Bulletin, 102(1), pp.77-102.

Jones, S. C. 1997. A Technique for Faster Pulse-Decay Permeability Measurements in Tight Rocks. Society of Petroleum Engineers (SPE) formation evaluation, 12 (01), p. 19-26.

Katz, A. J., and Thompson, A. H., 1987. Prediction of rock electrical conductivity from mercury injection measurements. Geophysical research, 92, p. 599-607.

Klinkenberg, L.J., 1941. The permeability of porous media to liquids and gases. Drill. Prod. Pract. 200e213.

Koehrer, B., Heymann, C., Prousa, F., Aigner, T., 2010. Multiple-scale facies and reservoir quality variations within a dolomite body– outcrop analog study from the Middle Triassic, SW German Basin. Marine and Petroleum Geology 27, 386– 411.

Kopaska-Merkel, D.C. and Amthor, J.E. 1988. Very high pressure mercury porosimetry as a tool in reservoir characterization, Carbonate Evaporite, 3, p.53–63.

Laubach, S.E., Lander, R.H., Criscenti, L.J., Anovitz, L.M., Urai, J.L., Pollyea, R.M., Hooker, J.N., Narr, W., Evans, M.A., Kerisit, S.N. and Olson, J.E., 2019. The role of chemistry in fracture pattern development and opportunities to advance interpretations of geological materials. Reviews of Geophysics, 57(3), pp.1065-1111.

Léonide, P., Fournier, F., Reijmer, J.J., Vonhof, H., Borgomano, J., Dijk, J., Rosenthal, M., van Goethem, M., Cochard, J. and Meulenaars, K., 2014. Diagenetic patterns and pore space distribution along a platform to outer-shelf transect (Urgonian limestone, Barremian–Aptian, SE France). Sedimentary Geology, 306, p.1-23.

Longman, M.W., 1980. Carbonate diagenetic textures from near surface diagenetic environments. AAPG bulletin, 64(4), p.461-487.

Lucia, F. J., 2004. Origin and petrophysics of dolomite pore space. In: Braithwaite, C.J., Rizzi, G. and Darke, G., 2004. The geometry and petrogenesis of dolomite hydrocarbon reservoirs. Geological Society, London, Special Publications, 235(1), p. 141-155.

Lucia, F. J., 2007, Carbonate reservoir characterization Springer-Verlag Berlin Heidelberg, 331 p.

Ma, S. and Morrow, N.R., 1996. Relationships between porosity and permeability for porous rocks. In International Symposium of the Society of Core Analysts, September (pp. 8-10).

Maerten, L., Gillespie, P. and Pollard, D.D., 2002. Effects of local stress perturbation on secondary fault development. Journal of Structural Geology, 24(1), p.145-153.

Maliva, R.G., Missimer, T.M., Clayton, E.A. and Dickson, J.A.D., 2009. Diagenesis and porosity preservation in Eocene microporous limestones, South Florida, USA. Sedimentary Geology, 217(1), p.85-94.

McPhee, C., Reed, J. and Zubizarreta, I., 2015. Core Analysis: A Best Practice Guide, Elsevier, 64, 852p.

Mohammed Sajed, O.K. and Glover, P.W.J., 2020. Dolomitisation, cementation and reservoir quality in three Jurassic and Cretaceous carbonate reservoirs in north-western Iraq. Marine and Petroleum Geology, p.104256.

Mohammed Sajed, O.K., Glover, P.W. and Collier, R.E.L., 2021. Reservoir quality estimation using a new ternary diagram approach applied to carbonate formations in north-western Iraq. Journal of Petroleum Science and Engineering, 196, p.108024.

Mohammed-Sajed, O.K. and Glover, P.W., 2022. Influence of anhydritisation on the reservoir quality of the Butmah Formation in north-western Iraq. Marine and Petroleum Geology, 135, p.105391.

Moore, C.H., 1989. Carbonate diagenesis and porosity, Developments in Sedimentology, 46, 338 p.

Moore, C. H., 2001. Carbonate reservoirs, porosity evaluation and diagenesis in a sequence stratigrphic framework, Developments in sedimentology, Netherland, 55, 444p.

Nader, F.H., 2017. Multi-scale quantitative diagenesis and impacts on heterogeneity of carbonate reservoir rocks (pp. 1-132). Springer International Publishing.

Porras, J. C., and Campos, O., 2001. Rock typing: A key approach for petrophysical characterization and definition of flow units, Santa Barbara Field, Eastern Venezuela Basin. Society of Petroleum Engineers, SPE-69458-MS.

Quan, L., Wang, G., Zhang, Y., Hao, F., Xu, R., Zhou, L. and Liu, Z., 2023. Early dolomitization and subsequent hydrothermal modification of the middle Permian Qixia Formation carbonate in the northwest Sichuan Basin. Geoenergy Science and Engineering, 221, p.211384.

Rashid, F., Glover, P.W.J., Lorinczi, P., Collier, R. and Lawrence, J., 2015a. Porosity and permeability of tight carbonate reservoir rocks in the north of Iraq. Journal of Petroleum Science and Engineering, 133, pp. 147-161.

Rashid, F., Glover, P.W.J., Lorinczi, P., Hussein, D., Collier, R. and Lawrence, J., 2015b. Permeability prediction in tight carbonate rocks using capillary pressure measurements. Marine and Petroleum Geology, 68, pp. 536-550.

Rashid, F., Glover, P.W.J., Lorinczi, P., Hussein, D. and Lawrence, J.A., 2017. Microstructural controls on reservoir quality in tight oil carbonate reservoir rocks. Journal of Petroleum Science and Engineering, 156, pp. 814-826.

Rashid, F., Hussein, D., Glover, P.W.J., Lorinczi, P. and Lawrence, J.A., 2022. Quantitative diagenesis: Methods for studying the evolution of the physical properties of tight carbonate reservoir rocks. Marine and Petroleum Geology, 139.

Rider, M.H. and Kennedy, M., 2018. The geological interpretation of well logs, 3rd edition, Rider-French Consulting Ltd, Sutherland, U.K., 440p.

Ross, E. R., 2011. Grain's Petrophysical handbook: online shareware petrophysics Training and Reference manual.

Rushing, J.A., Newsham, K.E., Lasswel,P.M. l, Cox, J.C., and Blasingame, T.A.2004. Klinkenberg-Corrected Permeability Measurements in Tight Gas Sands: Steady-State.Versus Unsteady-State Techniques. SPE 89867.

Rysak, B., Gale, J.F., Laubach, S.E. and Ferrill, D.A., 2022. Mechanisms for the generation of complex fracture networks: Observations from slant core, analog models, and outcrop. Frontiers in Earth Science, 10, p.463.

Sabouhi, M., Moussavi-Harami, R., Kadkhodaie, A., Rezaee, P. and Jalali, M., 2022. A new approach to Quantitative Diagenesis Modeling (QDM) by integrated facies, well logs and seismic attributes from the cenomanian-early Turonian Sarvak Formation, Abadan Plain, SW Iran. Journal of Petroleum Science and Engineering, 218, p.110943.

Schlumberger,1989. Log interpretation principles/applications, 228p.

Schlumberger, 1997. Log Interpretation Charts, Houston, Schlumberger Wireline and Testing. 193p.

Scholle, P., A., and D. Ulmer-Scholle, S., 2003. A colour guide to the petrography of carbonate rocks: grains, textures, porosity, diagenesis. American Association of Petroleum Geologists Bulletin, 77, Tulsa, Oklahoma, U.S.A.

Selley, R. C., 2000. Applied Sedimentology. 2nd edition, Academic press, 521p.

Shuja Ullah, Hanif, M., Radwan, A.E., Luo, C., Rehman, N.U., Ahmad, S., Latif, K., Ali, N., Thanh, H.V., Asim, M. and Ashraf, U., 2023. Depositional and diagenetic modeling of the Margala Hill Limestone, Hazara area (Pakistan): Implications for reservoir characterization using outcrop analogues. Geoenergy Science and Engineering, 224, p.211584.

Spain, D.R., 1992: Petrophysical evaluation of a slope fan/ basinfoor fan complex, cherry canyon formation, Ward County, Texas, AAPG Bulletin, 76 (6), p. 805-827.

Stentoft, N., Lapinskas, P. and Musteikis, P., 2003. Diagenesis of Silurian reefal carbonates, Kudirka oilfield, Lithuania. Journal of Petroleum Geology, 26(4), p.381-402.

Tavakoli, V., Rahimpour-Bonab, H. and Esrafili-Dizaji, B., 2011. Diagenetic controlled reservoir quality of south Pars gas field, an integrated approach. Comptes Rendus Geoscience, 343, p. 55- 71.

Tiab, D., and E. C. Donaldson, 2012. Petrophysics: Theory and practice of measuring reservoir rock and fluid transport properties 3rd edition. Elsevier, 950 p.

Tucker, M. E., V. P. Wright, and J. Dickson, 1990, Carbonate Sedimentology. Blackwell Science Ltd. 480p.

Verwer, K., Braaksma, H. and Kenter, J.A., 2008. Acoustic properties of carbonates: Effects of rock texture and implications for fluid substitution. Geophysics, 73(2), p.B51-B65.

Wang, M., Yang, Z., Shui, C., Yu, Z., Wang, Z. and Cheng, Y., 2019. Diagenesis and its influence on reservoir quality and oil-water relative permeability: A case study in the Yanchang Formation Chang 8 tight sandstone oil reservoir, Ordos Basin, China. *Open Geosciences*, *11*(1), pp.37-47.

Wang, Q., Narr, W. and Laubach, S.E., 2023. Quantitative characterization of fracture spatial arrangement and intensity in a reservoir anticline using horizontal wellbore image logs and an outcrop analogue. Marine and Petroleum Geology, p.106238.

Washburn, E. W., 1921. Note on a method of determining the distribution of pore sizes in a porous material. Proceedings of the National Academy of Sciences, 7, p. 115-116.

Wennberg, O.P., Casini, G., Jonoud, S. and Peacock, D.C., 2016. The characteristics of open fractures in carbonate reservoirs and their impact on fluid flow: a discussion. p. 91-104.

Worden, R.H., Armitage, P.J., Butcher, A.R., Churchill, J.M., Csoma, A.E., Hollis, C., Lander, R.H. and Omma, J.E., 2018. Petroleum reservoir quality prediction: overview and contrasting approaches from sandstone and carbonate communities. Geological Society, London, Special Publications, 435(1), pp.1-31.

Wyllie, M.R.J., Gregory, A.R. and Gardner, L.W., 1956. Elastic wave velocities in heterogeneous and porous media. Geophysics, 21(1), pp.41-70.

Zhang, M., Takahashi, M., Morin, R. H. and Esaki, T. 2000. Evaluation and Application of the Transient-Pulse Technique for Determining the Hydraulic Properties of Low-Permeability Rocks – Part 1: Theoretical Evaluation. American Society for Testing and Materials : Geotechnical Testing Journal, p.83-90.

Zhang, L., Jiao, Y., Rong, H., Li, R. and Wang, R., 2017. Origins and Geochemistry of Oolitic Dolomite of the Feixianguan Formation from the Yudongzi Outcrop, Northwest Sichuan Basin, China. Minerals, 7(120), p.1-21.

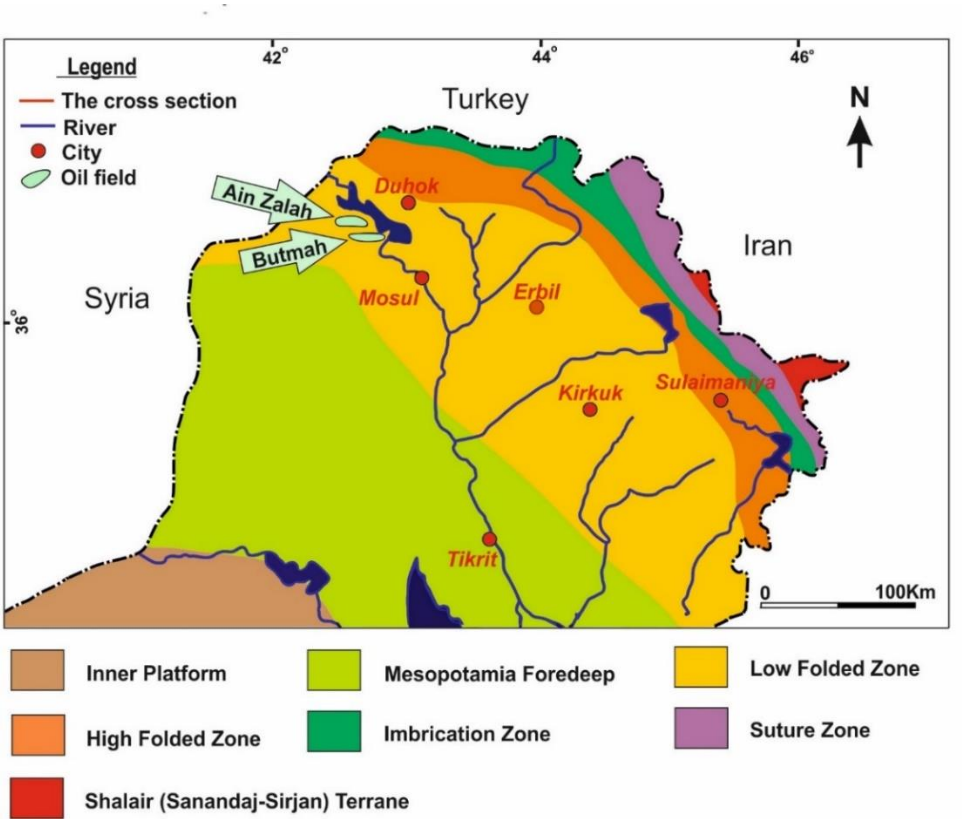

Figure 1. The position of the Butmah and Ain Zalah oilfields in north-western Iraq may be observed along with the tectonic division of Iraq after Fouad (2015).

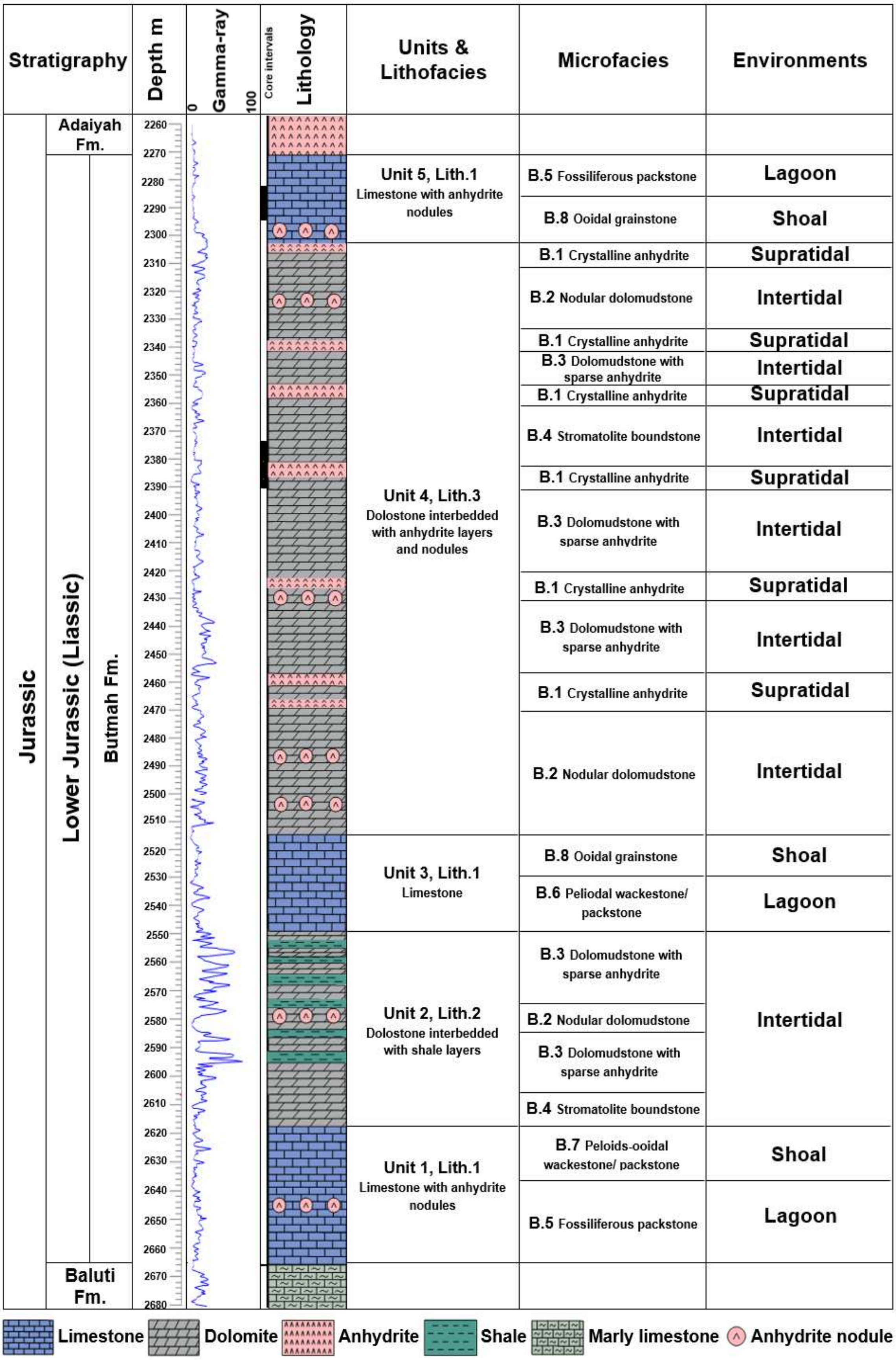

Figure 2. Stratigraphic units, lithofacies, microfacies distribution, and environments of the Butmah Formation at well Bm-15.

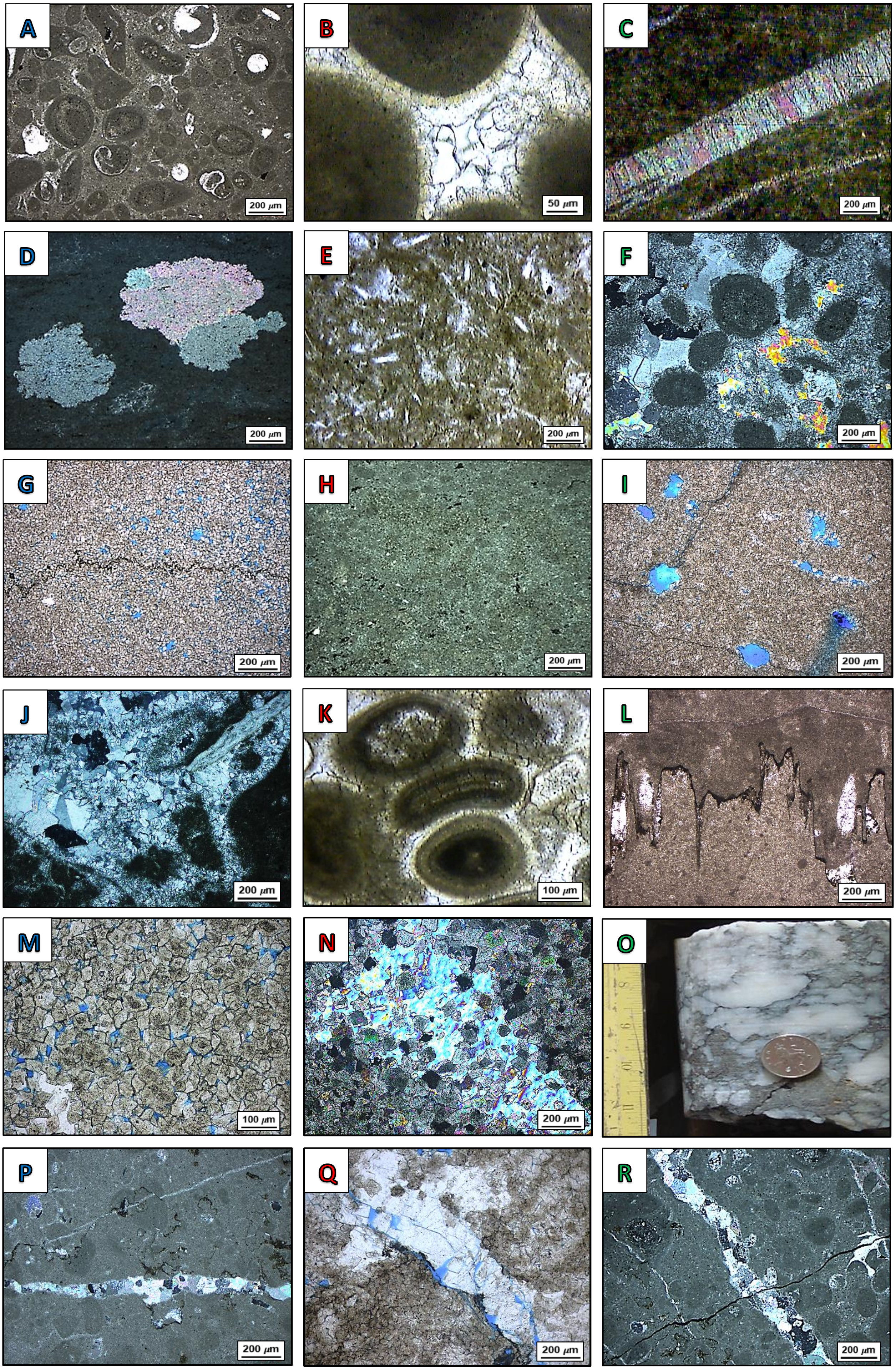
A
200 μm
B
50 μm
C
200 μm
D
200 μm
E
200 μm
F
200 μm
G
200 μm
H
200 μm
I
200 μm
J
200 μm
K
100 μm
L
200 μm
M
100 μm
N
200 μm
O
P
200 μm
Q
200 μm
R
200 μm

Figure 3. Observed textures associated with diagenetic processes. (A) Micritic envelops around skeletal grains (ooids), Bm-15, (2627 m). (B) Isopachous cement, Bm-15, (2540 m). (C) Fibrous cement, Bm-15, (2480 m). (C) Blocky cement, Bm-15, (2524 m). (D) Anhydrite nodules in fine dolomite crystals, Bm-15, (2500 m). (E) Spare anhydrite crystals in Dolomudstone microfacies, Bm-15, (2350 m). (F) Poikilotopic anhydrite cement, Bm-15, (2292 m). (G) A low peak amplitude stylolite (pressure solution) within fine crystalline dolomite, Bm-15, (2391m). (H) Slightly-compacted contacts between dolomitised peloids, Bm-15, (2541 m). (I) Fine crystalline dolomite showing vuggy porosity and solution-enlarged vugs Bm-15, (2391 m). (J) Drusy cement, Bm-15 (2290 m). (K) Mechanical compaction between ooids within ooids grainstone microfacies, Az-29, (3358 m). (L) A high peak amplitude stylolite (pressure solution) within fine crystalline dolomite, Bm-15, (2378m). (M) Zoning coarse dolomite crystals as late dolomitisation features, Bm-15, (2376 m). (N) Late-stage anhydrite cement occluding early porosity, Bm-15, (2390 m). (O) Compressed chicken-wire texture by compaction effect, Bm-15, (2379 m). (P) Late-stage blocky anhydrite cement fills some fractures and alongside stylolite, Bm-15, (2524 m). (Q) Burial dissolution as a few voids and solution enlarged stylolite, Bm-15, (2381 m). (R) Two generations of fractures, the old fracture is occluded by blocky anhydrite cement and the new open fracture cuts the old one, Bm-15, (2524 m).

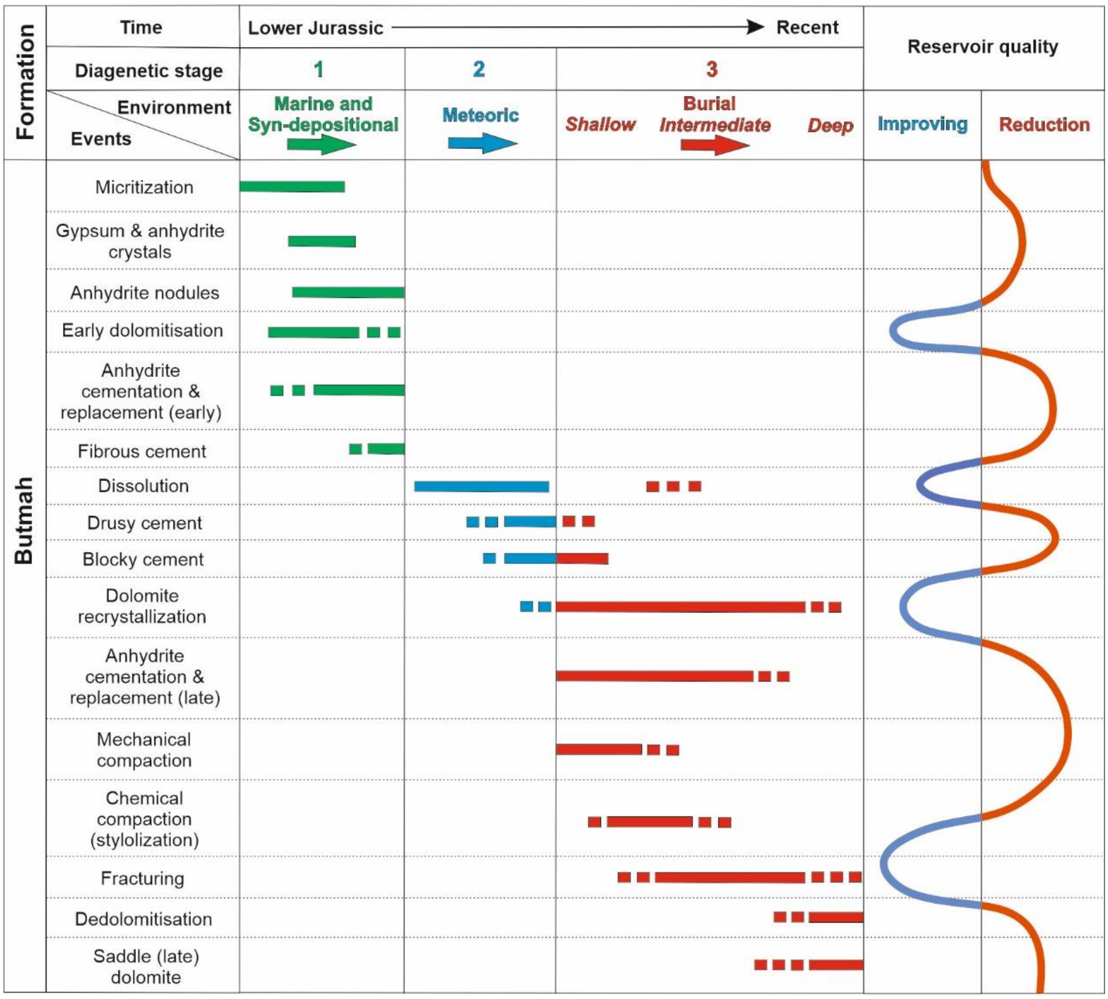

Figure 4. Summaries of the qualitative diagenetic pathway include a generalised diagenetic sequence with the effect of each diagenetic process on the reservoir quality of the Butmah Formation.

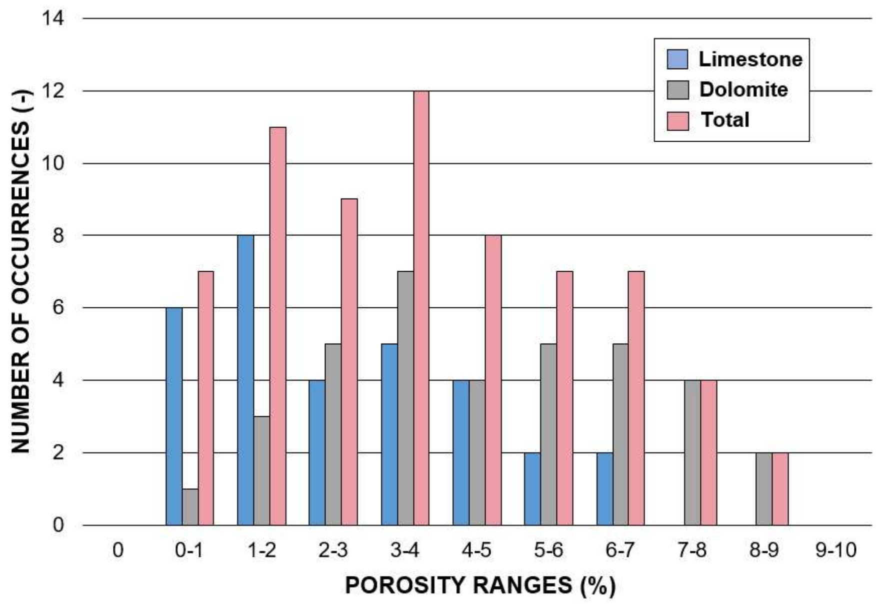

Figure 5. The effective porosity histogram of the Butmah Formation at well Bm-15.

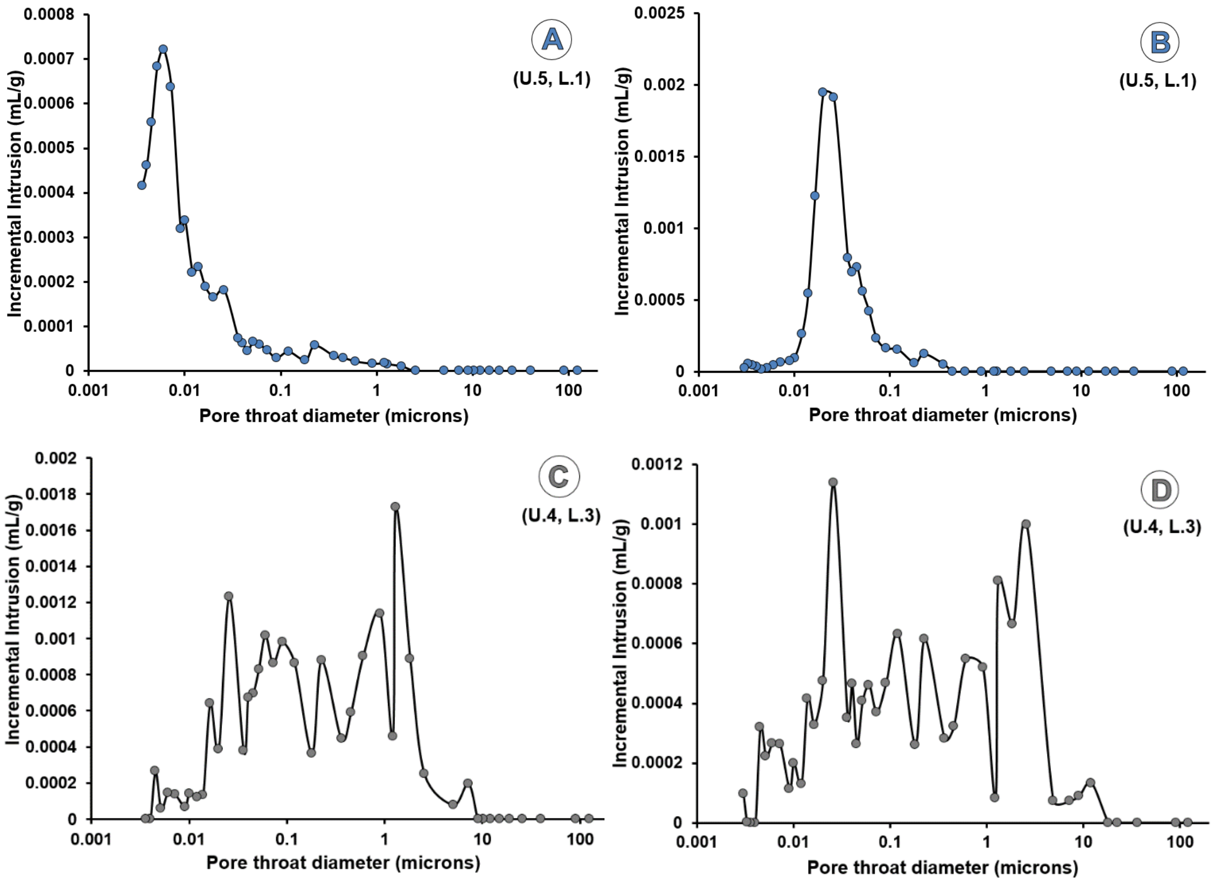

Figure 6. Pore throat distributions for four samples from the Butmah Formation; top row (A and B) from the limestone lithofacies (U5, L1), and bottom row (C and D) from the dolomite lithofacies (U4, L3).

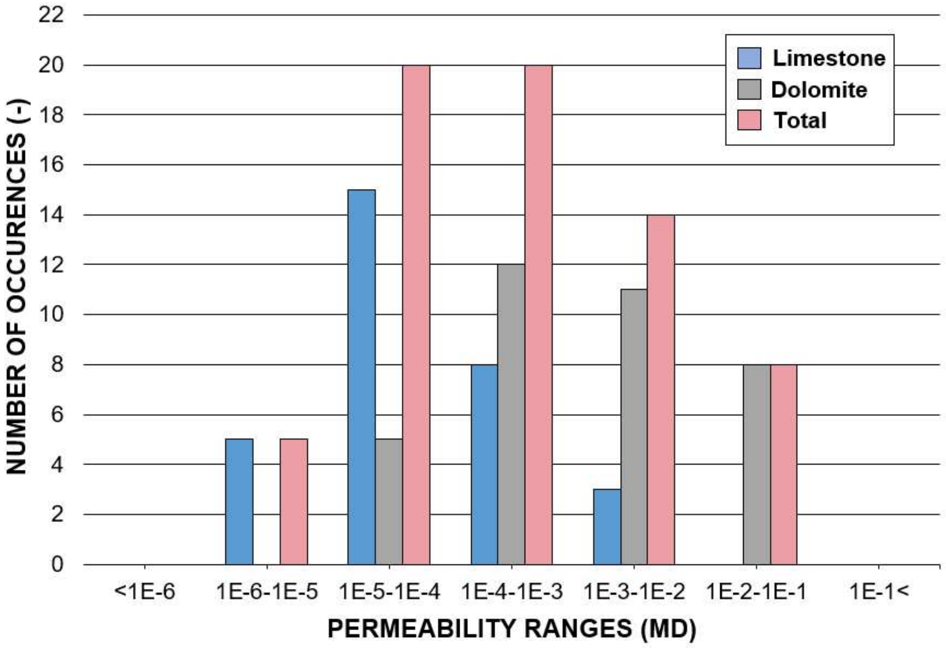

Figure 7. Histogram showing the permeability of the dolomite and limestone lithofacies in the Butmah Formation.

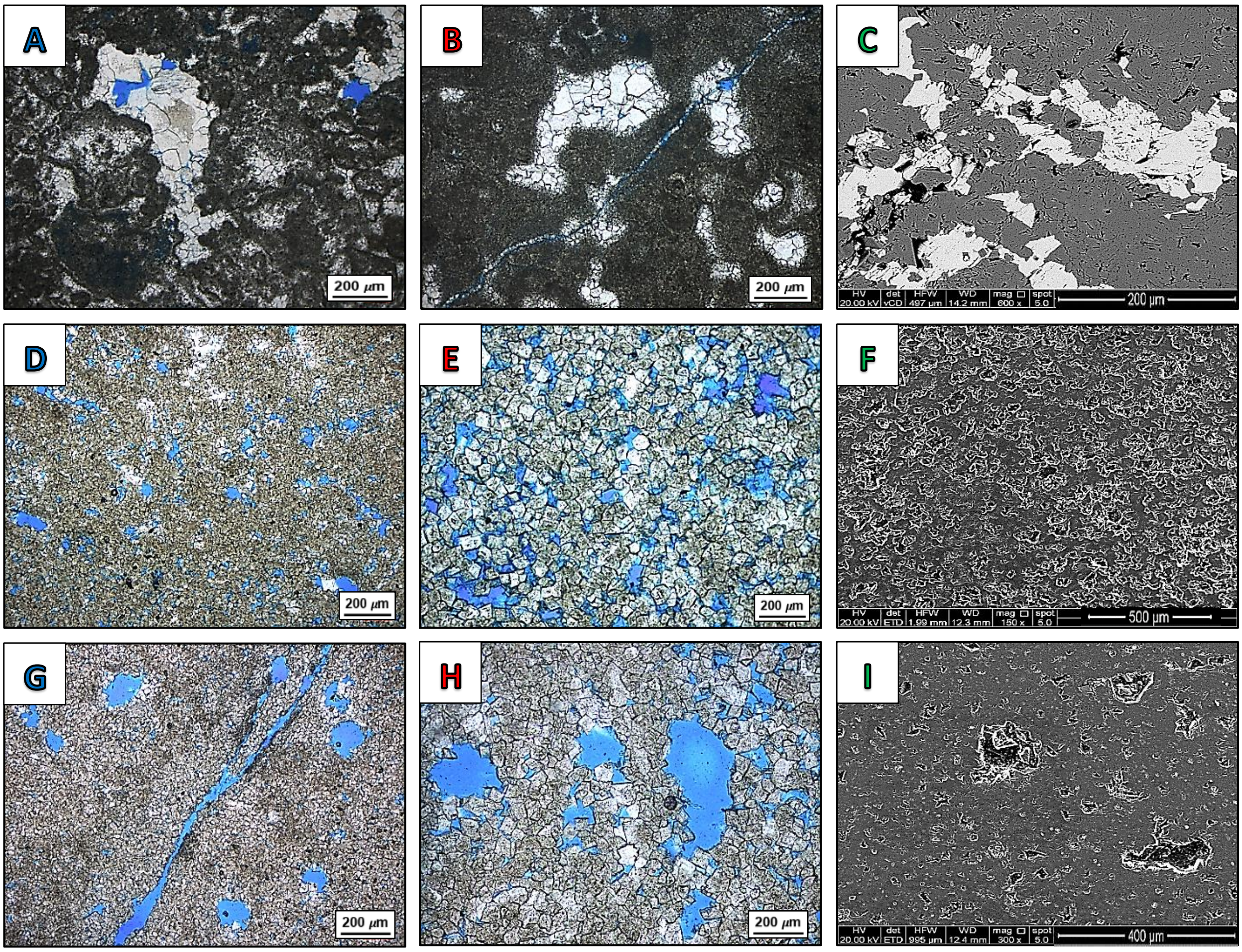

Figure 8. The Butmah Formation pore structures. (A) (B) (C) Stromatolite boundstone microfacies, Bm-15, U4 (2278 m) with (A) intercrystalline porosity and (B) intercrystalline and fracture porosity (C) SEM backscatter image illustrating pore space geometry, and anhydrite cement effects. (D) Fine crystalline dolomite with intercrystalline and vuggy porosity, Bm-15, U2 (2580 m). (E) Coarse crystalline dolomite of Lithofacies 3 showing intercrystalline porosity Bm-15, U4 (2391 m). (F) SEM images showing pores shape and size in coarse crystalline dolomite, Bm-15, U4 (2391 m). (G) Fine crystalline dolomite of lithofacies 3 showing vuggy and fracture porosity, Bm-15, U4 (2450 m). (H) Coarse crystalline dolomite showing intercrystalline porosity and solution-enlarged vugs Bm-15, U4 (2391 m). (K) SEM images showing intercrystalline and vuggy porosity in medium dolomite crystals, Bm-15, U4 (2388m).

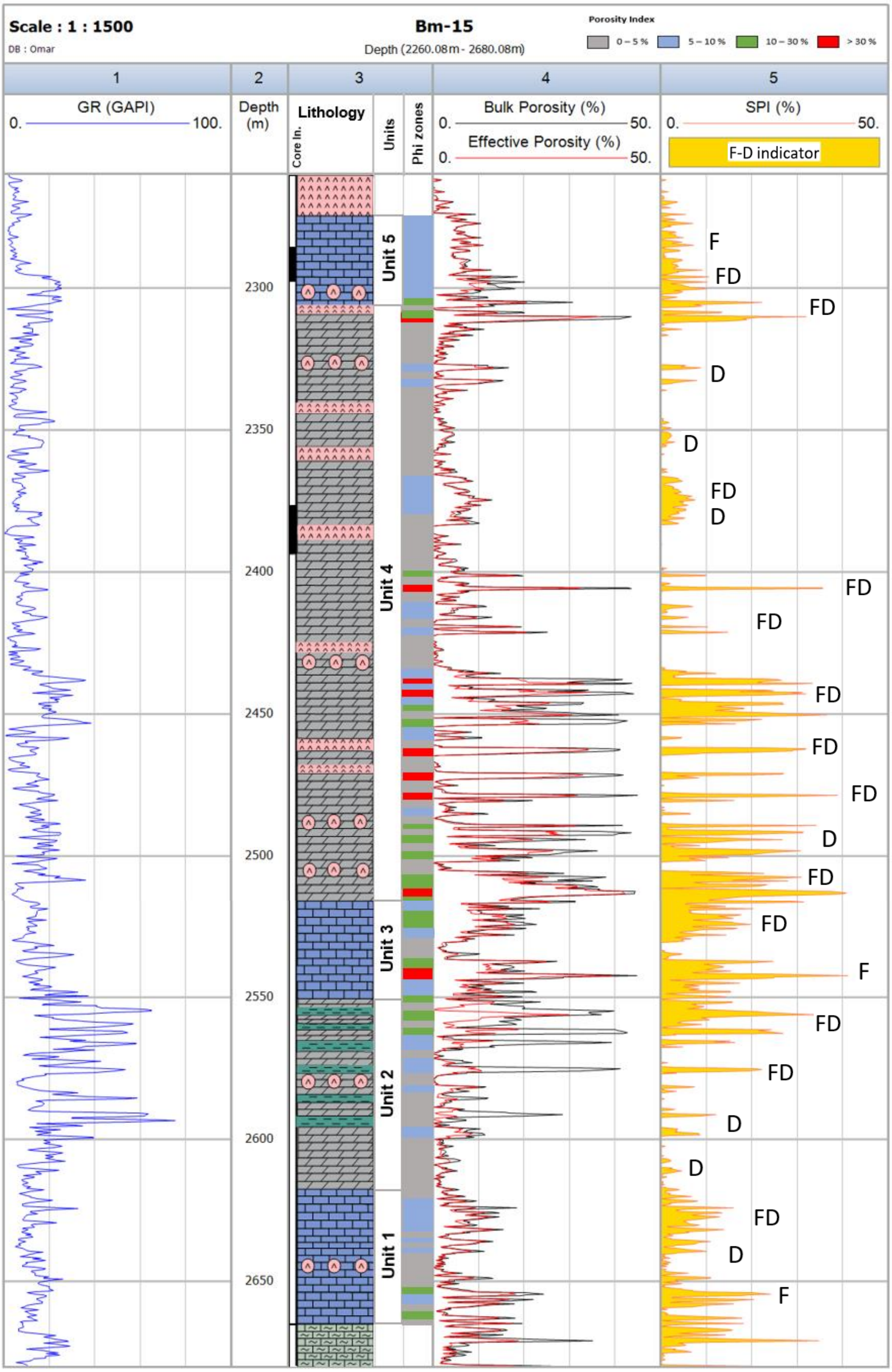

Figure 9. Porosity distribution (bulk and effective) within the Butmah Formation at well Bm-15 with secondary porosity indicator (SPI) and fracturing-diagenesis indicator (FDI) at each depth.

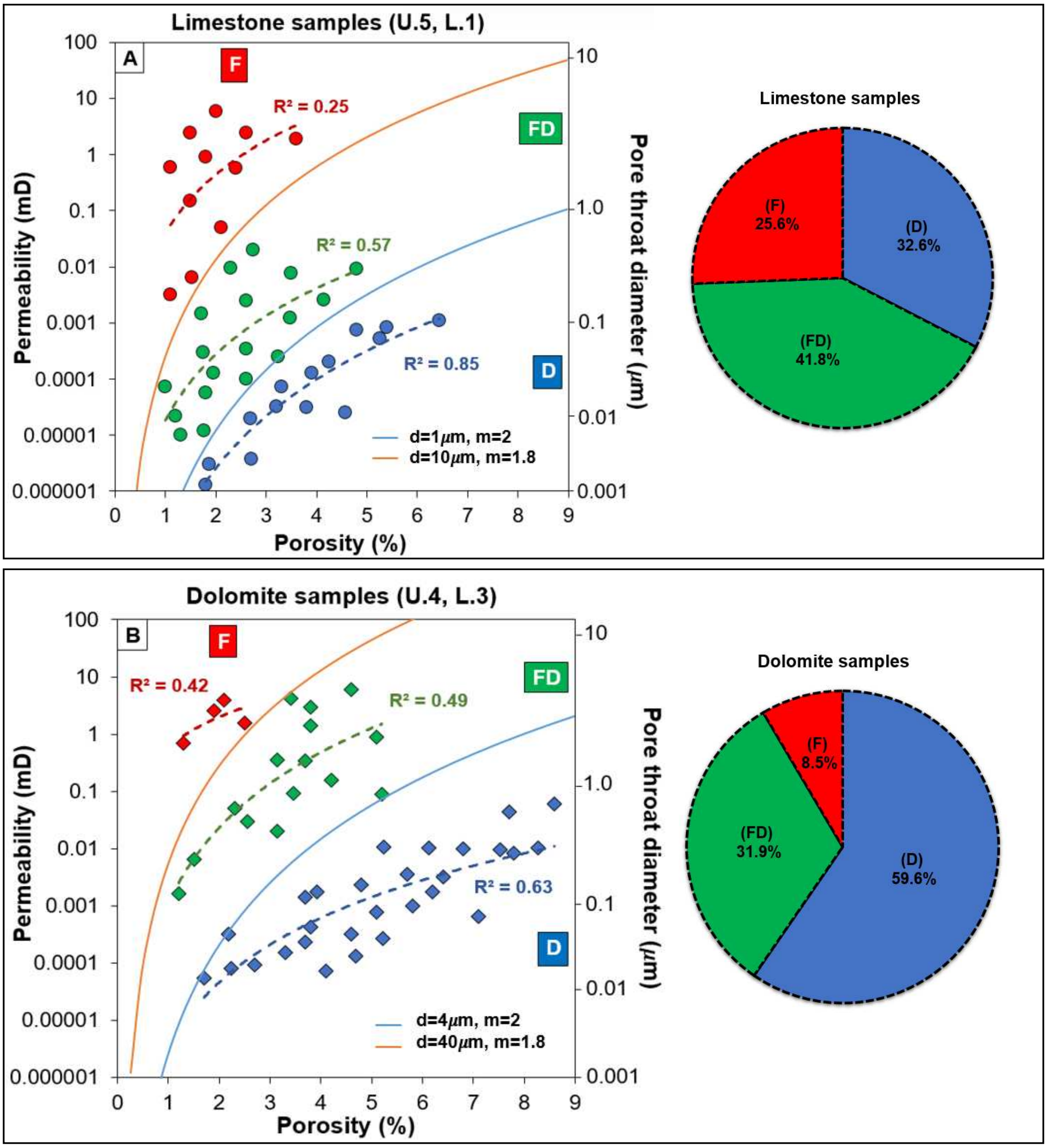

Figure 10. Porosity-permeability relationships with controlling factors shown as identified petrophysical fields. (A) The poroperm relationship for the limestone samples (U.5, L.1) with pie chart shows the distribution of the identified petrophysical fields. (B) The poroperm relationship for the dolomite samples (U.4, L.3) with pie chart shows the distribution of the identified petrophysical fields. The solid lines partitioning the poroperm relationships are RGPZ contours where the grain size (d) and cementation exponent (m) parameters are given in the figure (Glover et al., 2006; Rashid et al., 2015b). The dashed lines are best fit RGPZ-type power laws for each field.

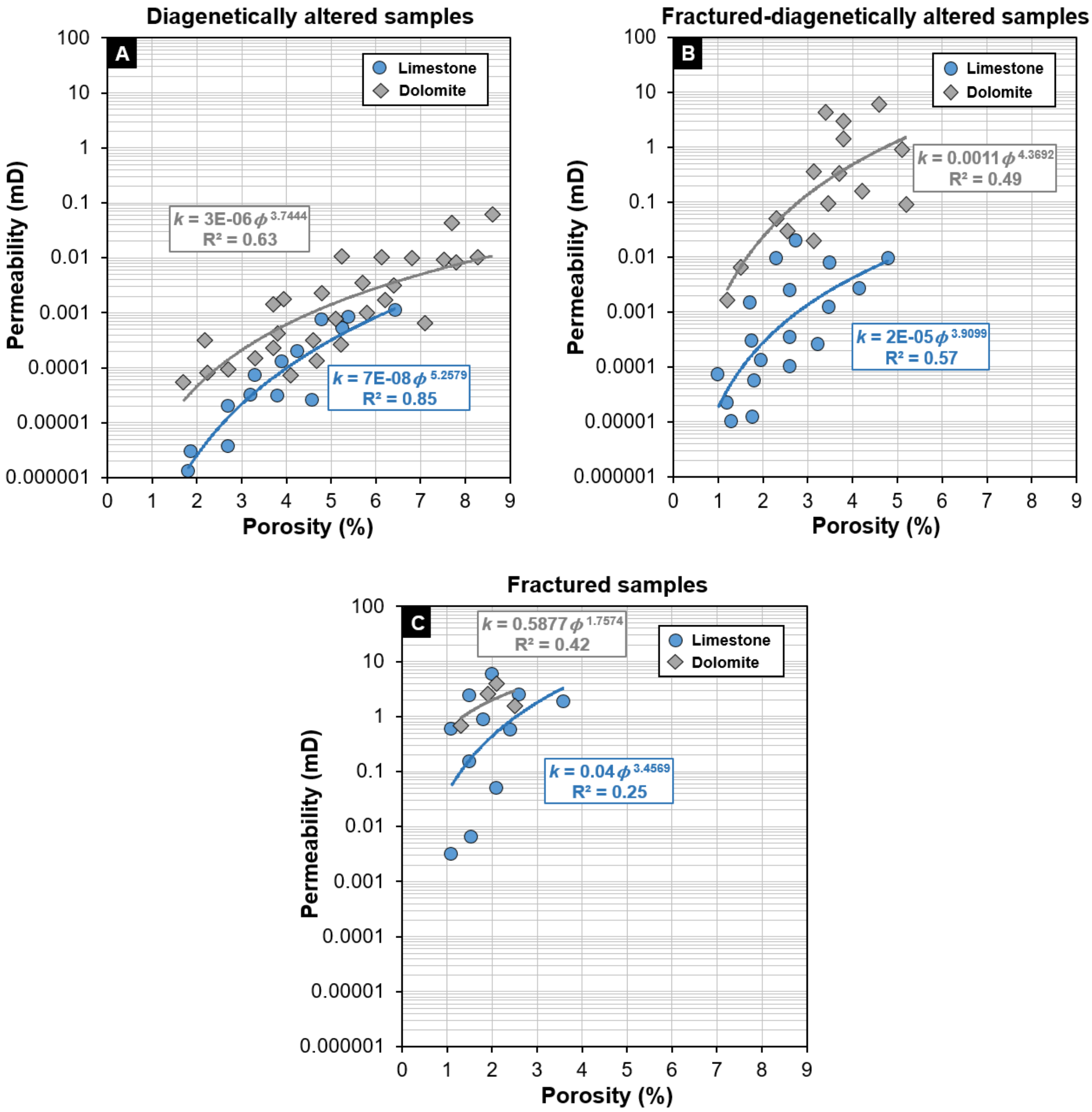

Figure 11. Comparison of the three identified petrophysical fields in both lithology limestone and dolomite including porosity, permeability, and the non-linear best fitting equations with a power law coefficient of determination (R^2). (A) Diagenetically altered samples. (B) Fractured and diagenetically- altered samples. (C) Fractured samples.

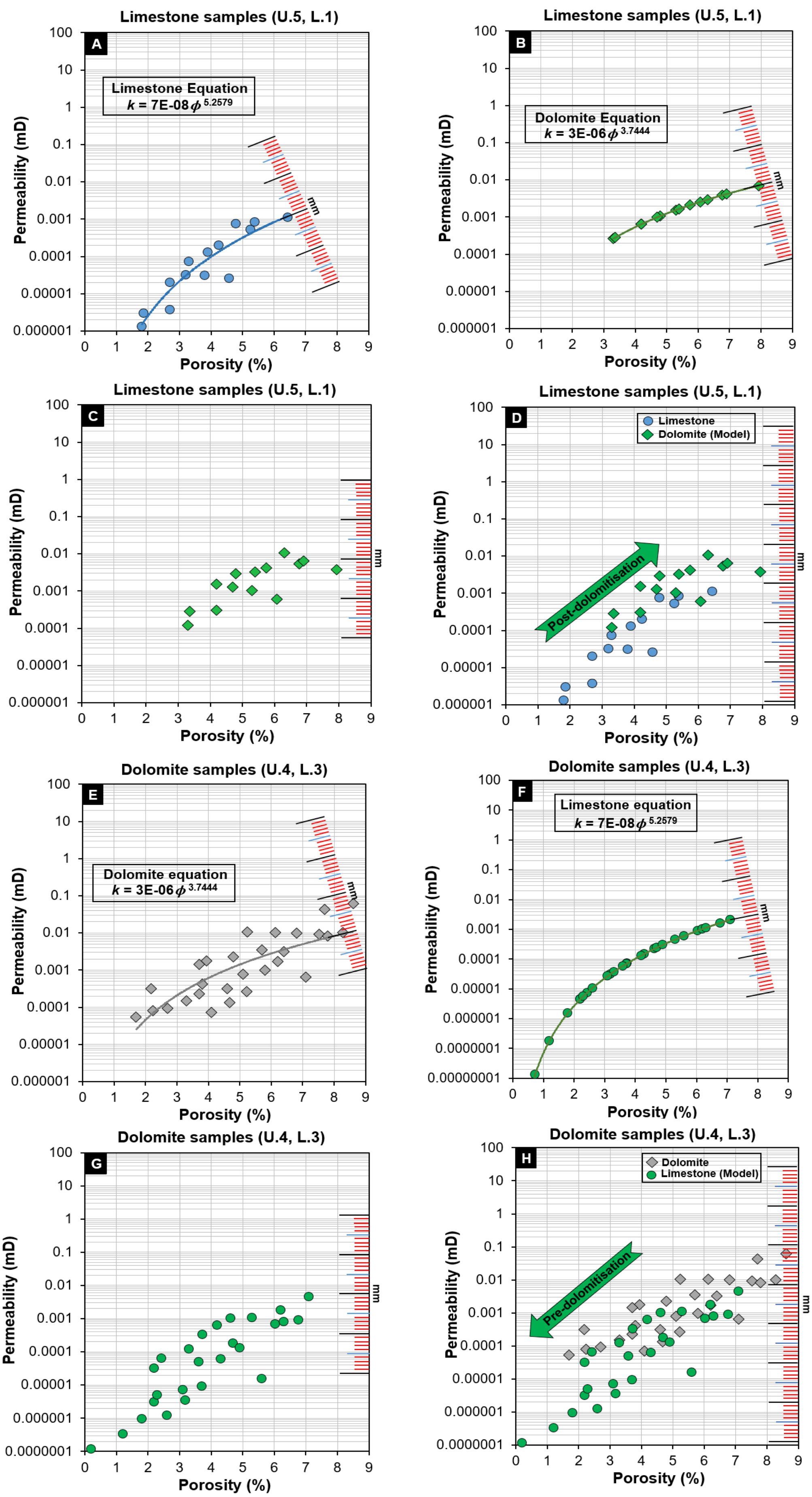

Figure 12. Prediction of post-dolomitisation dolomite poroperm data and the pre-dolomitisation limestone data for the diagenetic-altered samples (Field D). (A-D) The limestone samples (U.5, L.1) are used to estimate their post-dolomitisation petrophysical properties. (E-H) The dolomite samples (U.4, L.3) are used to estimate the pre-dolomitisation petrophysical properties.

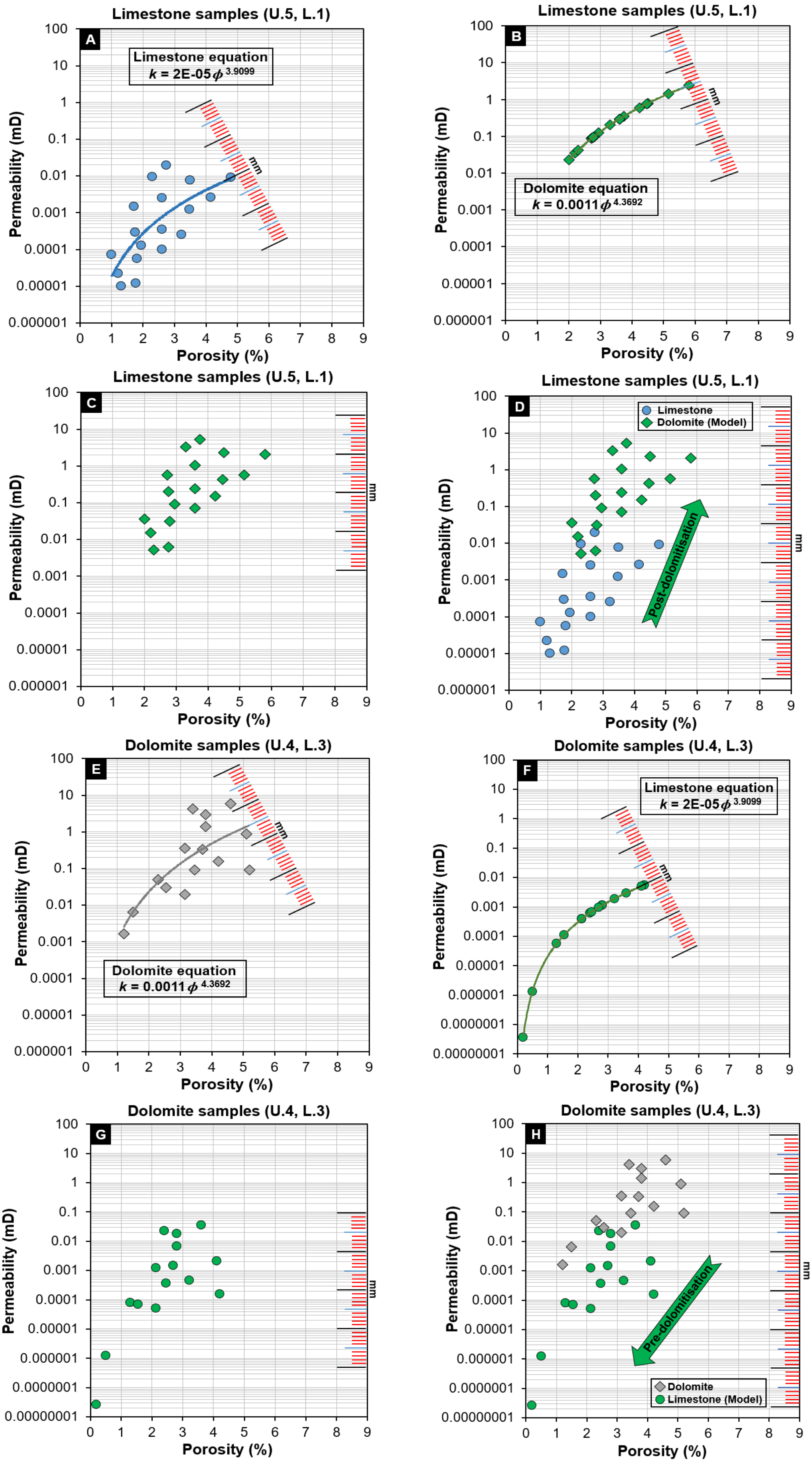

Figure 13. Prediction of post-dolomitisation dolomite poroperm data and the pre-dolomitisation limestone data for the fractured and diagenetically altered samples. (A-D) The limestone samples (U.5, L.1) are processes of estimating the post-dolomitisation petrophysical properties. (E-H) The dolomite samples (U.4, L.3) are processes of the pre-dolomitisation petrophysical properties.

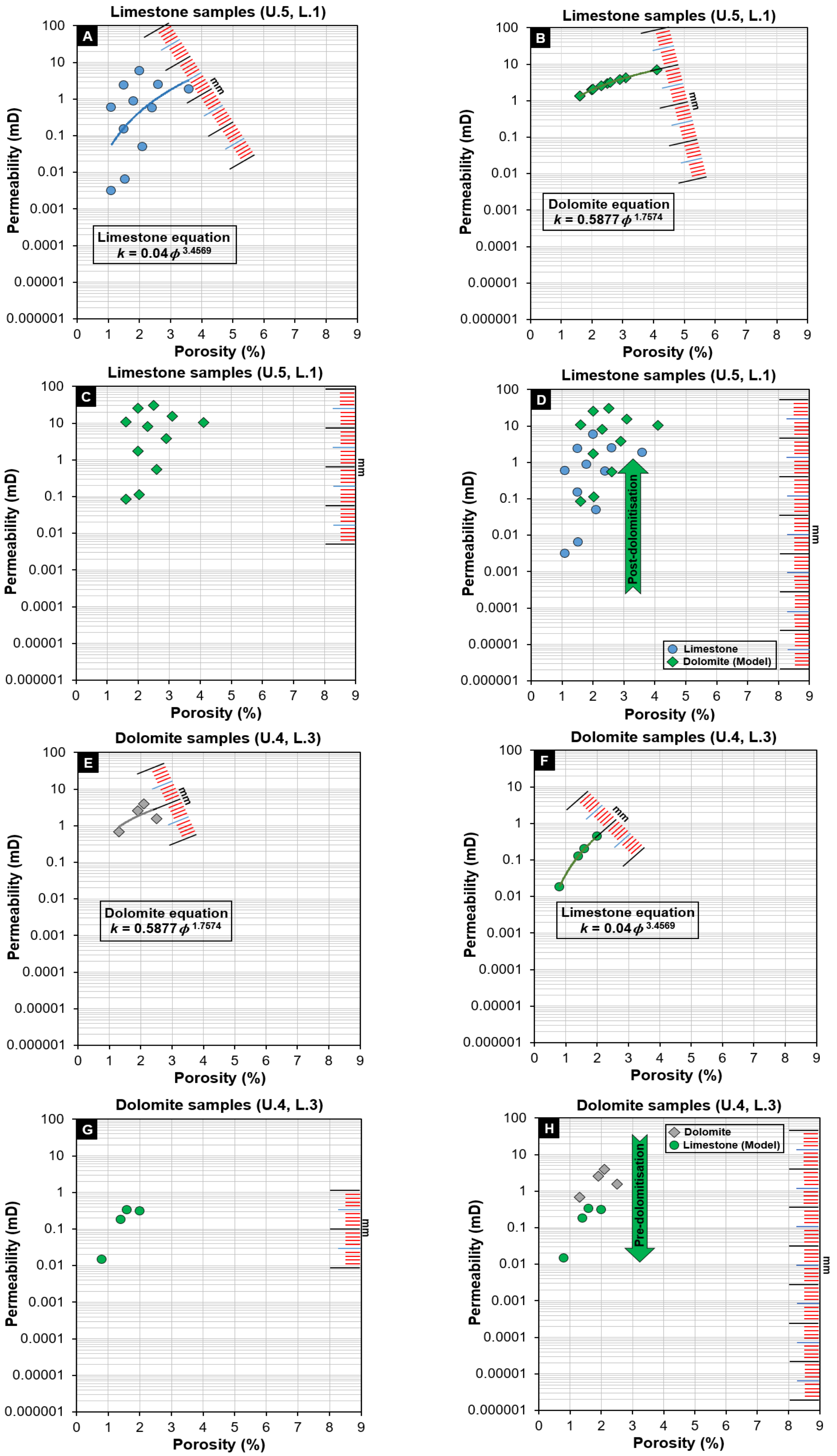

Figure 14. Prediction of post-dolomitisation dolomite poroperm data and the pre-dolomitisation limestone data for the fractured samples. (A-D) The limestone samples (U.5, L.1) are processes of estimating the post-dolomitisation petrophysical properties of limestone samples. (E-H) The dolomite samples (U.4, L.3) are processes of the pre-dolomitisation petrophysical properties.

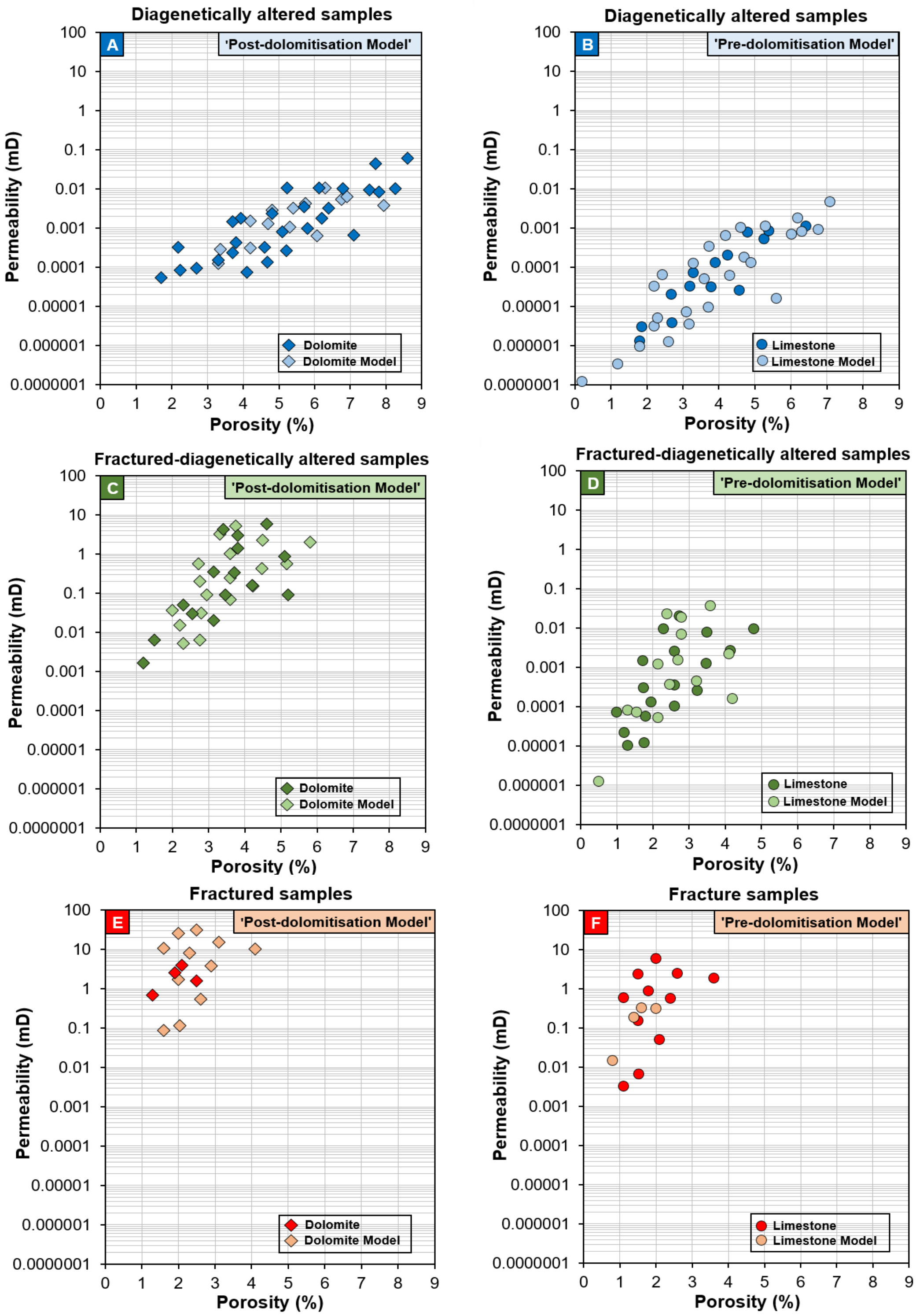

Figure 15. Comparison of the modelled post-dolomitisation and pre-dolomitisation porosity and measured permeability values with values from associated dolomite and limestones, respectively. (A) predicted and measured values for post-dolomitisation dolomite in diagenetic field samples (Field D), (B) predicted and measured values for pre-dolomitisation limestone in diagenetic field samples (Field D), (C) predicted and measured values for post-dolomitisation dolomite in fractured-diagenetic field samples (Field FD), (D) predicted and measured values for pre-dolomitisation limestone in fractured-diagenetic field samples (Field FD), (E) predicted and measured values for post-dolomitisation dolomite in fractured field samples (Field F), (F) predicted and measured values for pre-dolomitisation limestone in fractured field samples (Field F).

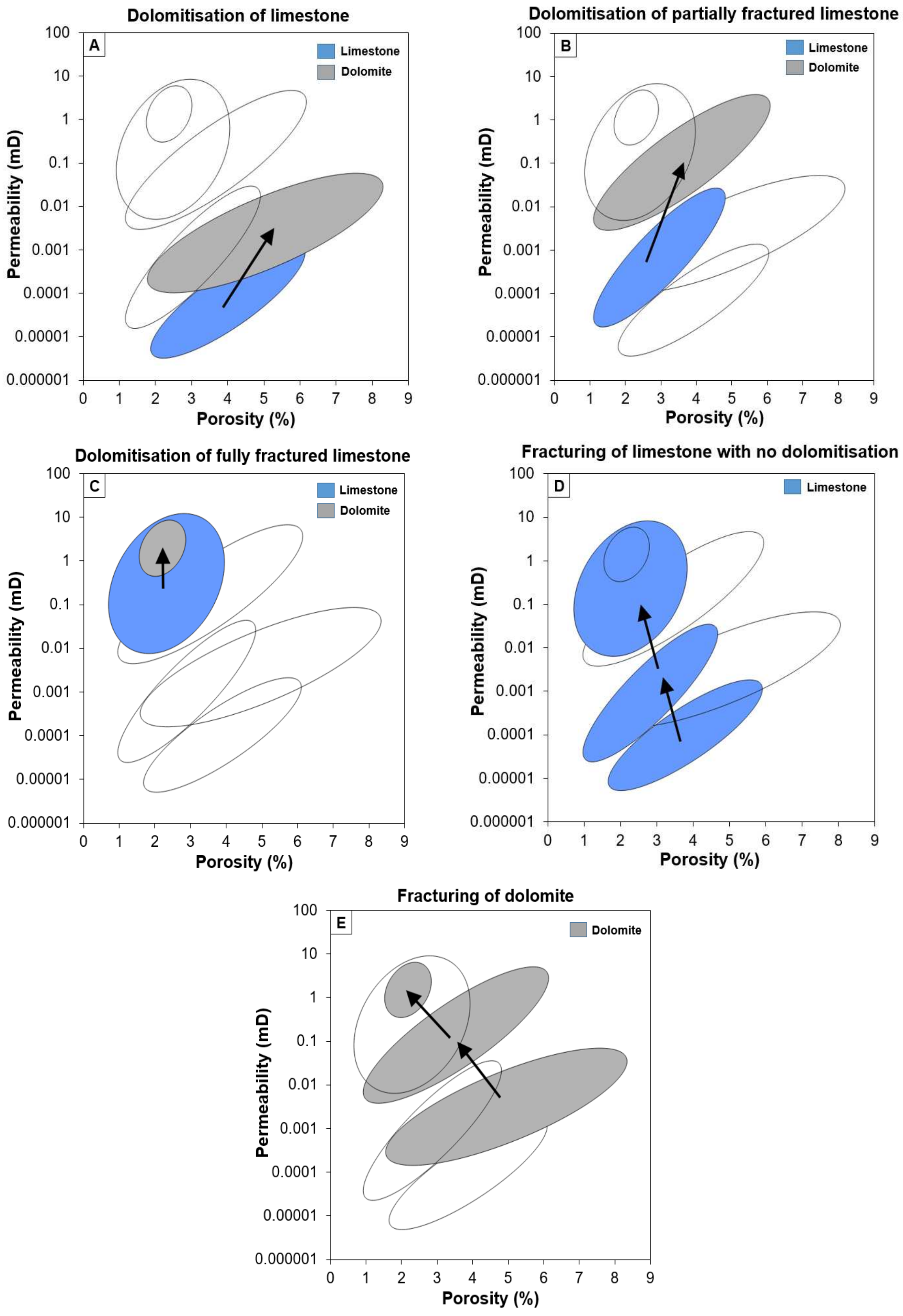

Figure 16. The petrodiagenetic pathway of the Butmah Formation according to the effect of dolomitisation and fracturing. (A) Dolomitisation of limestone. (B) Dolomitisation of partially fractured limestone. (C) Dolomitisation of fully fractured limestone. (D) Fracturing of limestone with no dolomitisation. (E) Fracturing of dolomite.

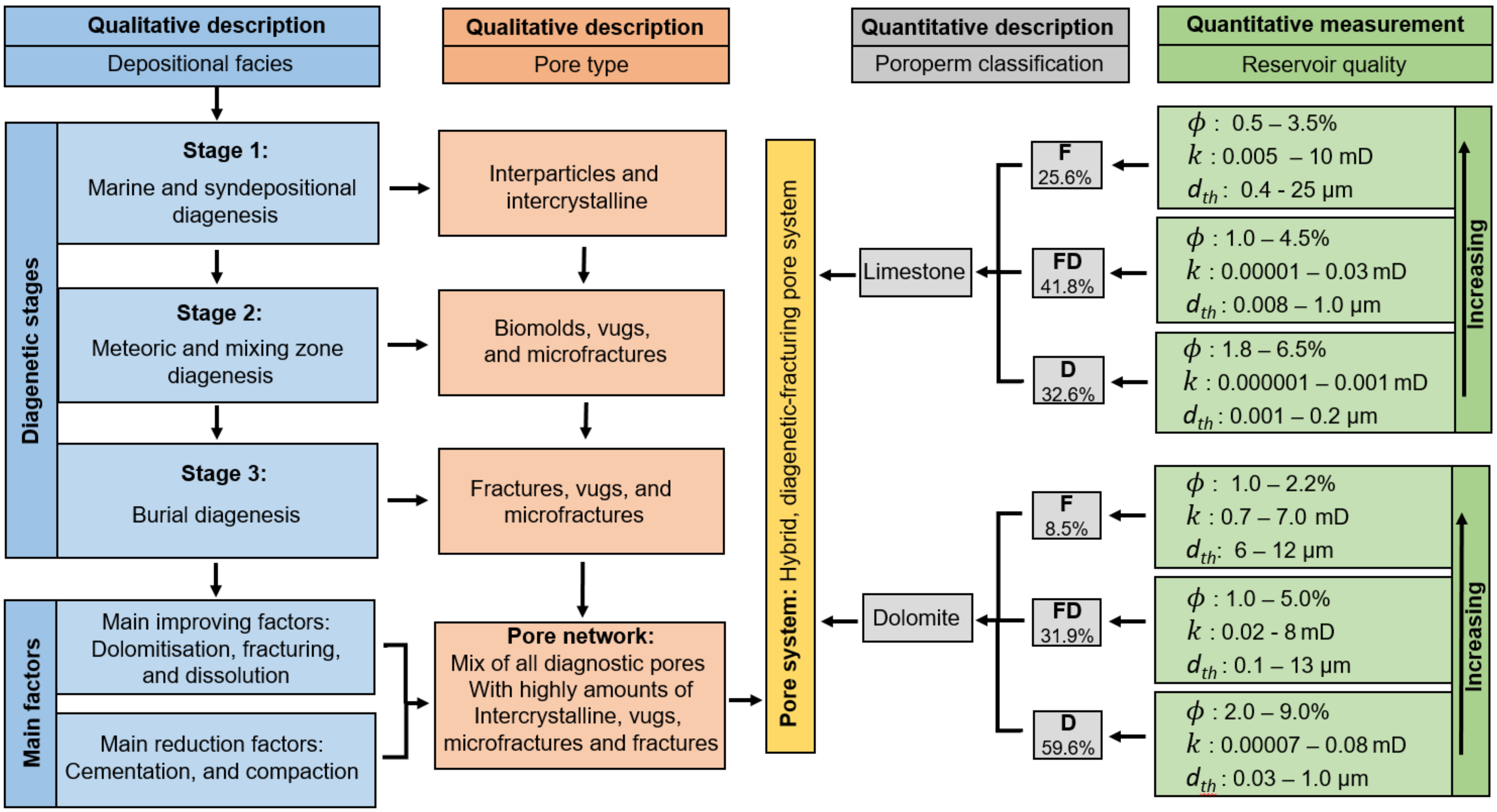

Figure 17. Flow chart summarising the qualitative and quantitative descriptions of the petrodiagenetic pathway of the Butmah Formation (ϕ, porosity; k, permeability; d_{th}, characteristic pore throat diameter).